Low-energy Coulomb excitation of ^{96,98}Sr beams

E. Clément, M. Zielinska, S. Péru, H. Goutte, S. Hilaire, A. Görgen, W. Korten, D. Doherty, B. Bastin, C. Bauer, et al.

Low-energy Coulomb excitation of ^{96,98}Sr beams

E. Clément,[1,2,*] M. Zielińska,[3,4] S. Péru,[5] H. Goutte,[3] S. Hilaire,[5] A. Görgen,[6] W. Korten,[3] D. T. Doherty,[3,7] B. Bastin,[1] C. Bauer,[8] A. Blazhev,[9] N. Bree,[10] B. Bruyneel,[9] P. A. Butler,[11] J. Butterworth,[7] J. Cederkäll,[2,12] P. Delahaye,[1,2] A. Dijon,[1] A. Ekström,[12] C. Fitzpatrick,[13] C. Fransen,[9] G. Georgiev,[14] R. Gernhäuser,[15] H. Hess,[9] J. Iwanicki,[4] D. G. Jenkins,[7] A. C. Larsen,[6] J. Ljungvall,[14] R. Lutter,[15] P. Marley,[7] K. Moschner,[9] P. J. Napiorkowski,[4] J. Pakarinen,[2] A. Petts,[11] P. Reiter,[9] T. Renstrøm,[6] M. Seidlitz,[9] B. Siebeck,[9] S. Siem,[6] C. Sotty,[14] J. Srebrny,[4] I. Stefanescu,[10] G. M. Tveten,[6,2] J. Van de Walle,[2] M. Vermeulen,[7] D. Voulot,[2] N. Warr,[9] F. Wenander,[2] A. Wiens,[9] H. De Witte,[10] and K. Wrzosek-Lipska[4]

[1]*GANIL, CEA/DRF-CNRS/IN2P3, F-14076 Caen Cedex 05, France*
[2]*PH Department, CERN 1211, Geneva 23, Switzerland*
[3]*Irfu, CEA, Université Paris-Saclay, F-91191 Gif-sur-Yvette, France*
[4]*Heavy Ion Laboratory, University of Warsaw, PL-02-093 Warsaw, Poland*
[5]*CEA, DAM, DIF, F-91297 Arpajon, France*
[6]*Department of Physics, University of Oslo, 0316 Oslo, Norway*
[7]*Department of Physics, University of York, YO10 5DD York, United Kingdom*
[8]*Institut für Kernphysik, Technische Universität Darmstadt, D-64289 Darmstadt, Germany*
[9]*Institute of Nuclear Physics, University of Cologne, D-50397 Cologne, Germany*
[10]*Instituut voor Kern-en Stralingsfysica, KU Leuven, Celestijnenlaan 200D, B-3001 Leuven, Belgium*
[11]*Oliver Lodge Laboratory, University of Liverpool, L69 7ZE Liverpool, United Kingdom*
[12]*Physics Department, University of Lund, Box 118, SE-221 00 Lund, Sweden*
[13]*Department of Physics, University of Manchester, M13 9PL Manchester, United Kingdom*
[14]*CSNSM, Université Paris-Sud, CNRS/IN2P3, Université Paris-Saclay, 91405 Orsay, France*
[15]*Fakultät für Physik, Ludwig-Maximilians-Universität München, D-85740 Garching, Germany*

(Received 22 September 2016; published 28 November 2016)

The structure of neutron-rich ^{96,98}Sr nuclei was investigated by low-energy safe Coulomb excitation of radioactive beams at the REX-ISOLDE facility, CERN, with the MINIBALL spectrometer. A rich set of transitional and diagonal $E2$ matrix elements, including those for non-yrast structures, has been extracted from the differential Coulomb-excitation cross sections. The results support the scenario of a shape transition at $N = 60$, giving rise to the coexistence of a highly deformed prolate and a spherical configuration in ^{98}Sr, and are compared to predictions from several theoretical calculations. The experimental data suggest a significant contribution of the triaxal degree of freedom in the ground state of both isotopes. In addition, experimental information on low-lying states in ^{98}Rb has been obtained.

DOI: 10.1103/PhysRevC.94.054326

I. INTRODUCTION

Neutron-rich, $A \sim 100$ nuclei are among the best examples of the interplay of microscopic and macroscopic effects in nuclear matter. A rapid onset of quadrupole deformation is known to occur at around $N = 60$ in the neutron-rich Zr and Sr isotopes, making this region an active area for both experimental and theoretical studies. Already in the 1960s, Johansson investigated properties of light fission fragments of ^{252}Cf and observed an island of large, constant deformation around A = 110 [1]. Later, mass measurements in this region of the nuclear chart showed that the binding energy of Rb, Sr, Y and Zr isotopes rapidly increases at $N = 60$ [2]. This onset of stability has been interpreted as a consequence of a dramatic increase of the ground-state deformation. The low-Z border of this phenomenon has been recently established by means of mass measurements in the Kr isotopic chain, where no deviation from the standard trend toward the drip line was observed at $N = 60$ [3]. The systematics of the excitation energy for the first 2^+ states in the Sr and Zr isotopic chains also show a sudden drop at $N = 60$, and by applying a simple geometrical model one can relate it to a change of deformation from $\beta_2 = 0.1$ to $\beta_2 = 0.4$. On the other hand, the energy of the first 2^+ state decreases smoothly between ^{94}Kr$_{58}$ and ^{96}Kr$_{60}$, consistent with the evolution of their masses, which confirms the local character of this phenomenon [4] and suggests that it is related to the interaction between specific proton and neutron orbitals. Finally, low-lying 0^+ states, indicating possible shape coexistence [5], have been identified in the Zr and Sr chains and, similar to the 2^+_1 state, an abrupt drop of the 0^+_2 energy is observed at $N = 60$. A shape coexistence scenario was, therefore, proposed, where the 0^+_2 states for $N < 60$ correspond to a deformed configuration, which then becomes the ground state at $N = 60$, while the spherical configuration of the ground state for $N < 60$ becomes non-yrast.

*clement@ganil.fr

Shape coexistence phenomena [5] represent some of the most striking changes in nuclear structure observed in either particular atomic nuclei or between neighbors of an isotopic chain. They are often associated with islands of inversion, where spherical configurations, corresponding to doubly-closed shells, compete with deformed configurations. In the deformed shell model approach, the onset of collectivity beyond $N = 58$ can be understood as a result of the competition between the spherical gaps at $Z = 38,40$ and $N = 56$, and the deformed subshell closures at $Z = 38,40$ and $N = 60, 62$, and 64. In the Sr and Zr isotopic chains, a spherical-to-deformed transition takes place when going from 58 to 60 neutrons, thus when the $\nu g_{7/2}$ orbital is being filled. Shell model calculations were performed for the Zr isotopic chain in an extended model space [6,7] and pointed to the π-ν interaction between the spin-orbit partners $\pi 0g_{9/2}$ and $\nu 0g_{7/2}$ as the main mechanism for the shape change: as the $\nu 0g_{7/2}$ orbital is being filled, the $Z = 40$ subshell gap between the $\pi 0f_{5/2}$ and $\pi 0g_{9/2}$ effective single-particle energies (ESPE) is reduced, giving rise to multiple particle-hole excitations across the gap. In the calculations, the 0_2^+ states below $N = 60$ result from two-particle–two-hole (2p-2h) proton excitations (with a possible 4p-4h contribution) from the pf shell into the $\pi 0g_{9/2}$ orbital. A similar mechanism is known to be responsible for the rapid onset of deformation and shape coexistence in neutron-rich isotopes around $N = 20$, 28, and 40, with different spin-orbit partners [5,8,9].

The structure of neutron-rich Sr isotopes beyond the first 2^+ state has been studied extensively in the past. In ^{96}Sr, the ground-state band was shown to have a vibrational-like character, and the small $B(E2; 2_1^+ \rightarrow 0_1^+)$ value extracted from the lifetime of 7(4) ps [10] is consistent with a nearly spherical ground state. Two low-lying 0^+ states at 1229 and 1465 keV were established by Jung *et al.* [11] and interpreted as candidates for a deformed band head, supporting the shape coexistence scenario. An extremely strong electric monopole transition of $\rho^2(E0) = 0.185(50)$ was observed between these two states [12,13], indicating the presence of a sizable deformation and strong mixing between the configurations. In ^{98}Sr, the ground-state band has a rotational character, and the large $B(E2)$ values between its members, deduced from lifetime measurements [10,14–19], are consistent with a deformed character of the ground state. A low-lying 0_2^+ state at 215.3 keV was established by Schussler *et al.* [20] and interpreted as the band head of a presumably spherical structure. A strong electric monopole transition of $\rho^2(E0) = 0.053(5)$ was measured between the 0_2^+ and the 0_1^+ states, again supporting the shape coexistence scenario [20,21].

We reported in a recent Letter on the spectroscopic quadrupole moments and reduced transition probabilities in ^{96,98}Sr measured by low-energy Coulomb excitation of post-accelerated radioactive ion beams at REX-ISOLDE, which provided firm evidence for shape coexistence and configuration inversion in the neutron-rich Sr isotopes [22,23]. In the present paper, we give a more in-depth description of the experiments, the data analysis procedures, and the theoretical calculations performed using the Gogny D1S interaction in a five-dimensional Hamiltonian. We also present detailed comparisons of measured transition strengths in ^{96,98}Sr with several other model predictions. The paper is organized as follows: the experiments are described in Sec. II, the data analysis is presented in Sec. III A for ^{96,98}Sr and in Sec. III B for a beam contaminant, ^{98}Rb, and the determination of electromagnetic matrix elements from Coulomb excitation data is presented in Sec. IV. The results are discussed in Sec. V. Finally, the conclusions of this work are summarized in Sec. VI.

II. EXPERIMENTAL DETAILS

Post-accelerated radioactive beams of ^{96}Sr and ^{98}Sr were delivered by the REX-ISOLDE facility at CERN with average intensities of 7×10^3 pps (particles per second) at 275.5 MeV and 6×10^4 pps at 276.3 MeV, respectively, to the Coulomb excitation setup of the MINIBALL high-purity germanium (HPGe) detector array [24]. Several different targets were used for this study in order to exploit the dependence of the Coulomb excitation cross section on the atomic numbers of the collision partners: ^{109}Ag (of thickness 1.9 mg/cm^2) and ^{120}Sn (2.0 mg/cm^2) in the case of ^{96}Sr, ^{60}Ni (2.1 mg/cm^2) and ^{208}Pb (1.45 mg/cm^2) for ^{98}Sr. The scattered Sr ions and recoiling target nuclei were detected with an annular double-sided silicon strip detector (DSSSD) covering an angular range from 20 to 55 degrees in the laboratory frame, which corresponds to 54°–166°, 37.5°–139.9°, 35.9°–139.9°, and 29.2°–139.9° in the center-of-mass (CM) system for the ^{60}Ni, ^{109}Ag, ^{120}Sn, and ^{208}Pb targets, respectively. Deexcitation γ-ray spectra were sorted in prompt coincidence with scattered particles detected in the annular silicon strip detector. Cline's safe energy criterion [25], ensuring a purely electromagnetic process, was fulfilled for all angles covered by the particle detector for scattering on the Ag, Sn, and Pb targets, while for the ^{60}Ni target center-of-mass angles above 112.9° degrees had to be excluded from the analysis. Doppler correction was applied on an event-by-event basis using both the position information from the particle detector and the electric segmentation of the MINIBALL detectors.

Two different methods of beam purification were used for ^{96}Sr and ^{98}Sr in order to suppress the strong isobaric contamination of rubidium. A pure ^{96}Sr beam was delivered thanks to molecular extraction of ^{96}Sr ^{19}F$^+$ from the primary UC$_x$ target. The HRS mass separator was set to the mass of the molecule ($A = 115$) and the ^{96}SrF beam was transferred to the EBIS charge breeder, where the molecules were broken up in the electron beam. The A/Q spectrometer, installed between the charge breeder and the REX linear accelerator, was tuned to $A/Q = 4.17$ in order to suppress the ^{115}In contamination stemming from the HRS setting. The beam composition was monitored by using the Bragg chamber developed within the MINIBALL Collaboration that provides mass (A) and element number (Z) for heavy ions of below mass $A \simeq 130$ [24]. The calibration of the Bragg chamber was validated using a stable ^{88}Sr beam. In the second experiment, the ^{98}Sr secondary beam was produced using the in-trap β-decay technique developed at REX-ISOLDE [26]. Among the $A = 98$ isobars that were extracted from the UC$_x$ primary target, the short-lived ^{98}Rb was found to be by far most intense, amounting to 95% of the total intensity. The ions were collected and cooled in

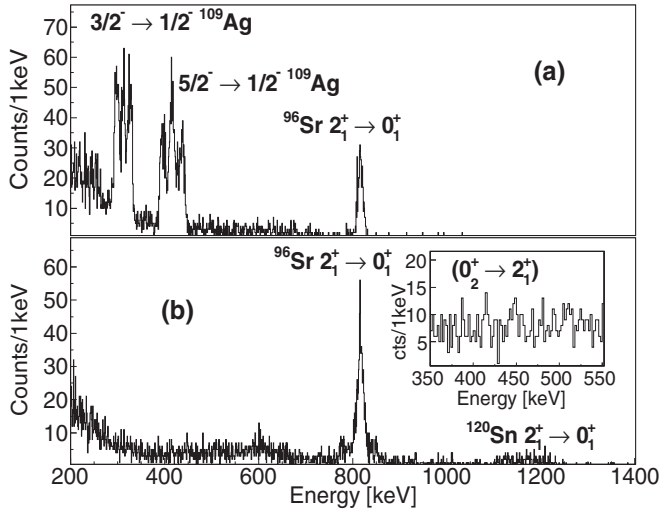

FIG. 1. (a) Total γ-ray spectrum from MINIBALL, following Coulomb excitation of the ^{96}Sr beam impinging on the ^{109}Ag target, Doppler corrected for the projectile. (b) Same spectrum for the excitation of ^{96}Sr on the ^{120}Sn target. The inset shows a zoom on the weak $0_2^+ \rightarrow 2_1^+$ transition.

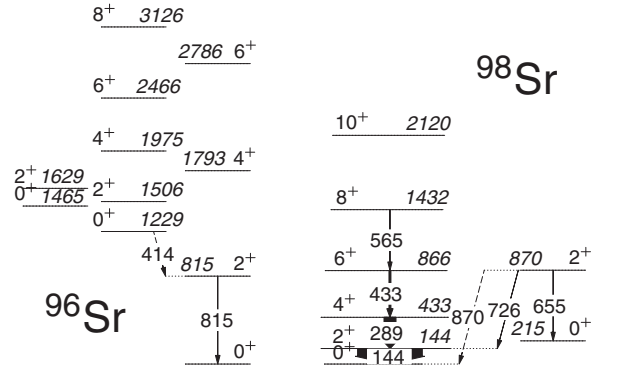

FIG. 2. Partial level schemes of ^{96}Sr (left) and ^{98}Sr (right), showing the transitions observed in the present measurement. Transition and level energies are given in keV. Arrow widths reflect the total measured intensities. The intensity of the transition at 870 keV, marked with a dashed arrow, was too low to be included in the Coulomb excitation analysis (see Sec. IV).

the REX-TRAP for 161 ms and then charge boosted in the EBIS charge breeder for 158 ms. The average processing time exceeded the half-life of ^{98}Rb ($T_{1/2} = 114(5)$ ms [27]) by a factor of 2, therefore, most of the ^{98}Rb nuclei decayed in trap to ^{98}Sr. The beam composition after post-acceleration was monitored using a ΔE-E detector consisting of a low-pressure ionization chamber and a silicon detector [24], and was determined consistently to be 5% ^{98}Rb, 80% ^{98}Sr, 15% ^{98}Y for mass $A = 98$. Other weak, stable contaminants which originate from the EBIS were also identified: $^{15}N^{4+}$, $^{64}Ni^{17+}$, $^{64}Zn^{17+}$, and $^{83}Kr^{22+}$; however, they amounted to less than 7% of the total beam intensity.

III. DATA ANALYSIS AND RESULTS

A. ^{96,98}Sr

The γ-ray spectra following Coulomb excitation of the ^{96}Sr beam are presented in Fig. 1. In both spectra, the $2_1^+ \rightarrow 0_1^+$ transition in ^{96}Sr is present at 815 keV, together with target excitation at 1171 keV for ^{120}Sn and 311 and 415 keV for ^{109}Ag. For the ^{120}Sn target, where the level of statistics is greater, an additional weak transition corresponding to the 0_2^+ decay was observed at 414 keV, as shown in the inset. A partial level scheme of ^{96}Sr is presented in Fig. 2, showing the transitions considered in the Coulomb excitation analysis.

In order to determine matrix elements from the differential Coulomb excitation cross section, the data collected on the ^{120}Sn target were divided into three subsets corresponding to different ranges of scattering angles. The γ-ray intensities extracted for each of the data sets are summarized in Table I. It should be noted that the decay of the 0_2^+ state, populated in a two-step excitation process, was observed only at high CM angles, and even then the corresponding transition was at the detection limit. The relative precision of the $0_2^+ \rightarrow 2_1^+$ intensity in coincidence with the particles scattered in the entire angular range covered by the silicon detector does not improve as compared to that obtained only for high CM angles (Table I).

The γ-ray spectra following Coulomb excitation of the ^{98}Sr beam are presented in Fig. 3. The rotational ground-state band was populated up to spins 6^+ and 8^+ using ^{60}Ni and ^{208}Pb targets, respectively. The decay of the 2_2^+ state via transitions at 655, 726, and 870 keV was also observed. The Doppler-broadened $2_1^+ \rightarrow 0_1^+$ transition in ^{60}Ni is visible at 1332.5 keV. Excitation of the ^{208}Pb target was too weak to be observed, but the Pb x rays are present in the spectrum at 72 and 75 keV. Several unknown transitions, marked with asterisks, are present in the spectra. Their origin is discussed in Sec. III B.

The 144-keV γ-ray line, corresponding to the 2_1^+ decay, exhibits additional structures on both the low- and high-energy sides. This is due to the fact that the lifetime of the 2_1^+ state [$T_{1/2} = 2.78(8)$ ns] [14] is comparable to the time of flight between the target and the annular silicon detector. Hence, part of the 2_1^+ decay occurs in flight and is properly Doppler corrected, while certain γ quanta are emitted after the ^{98}Sr

TABLE I. Observed γ-ray transitions in ^{96}Sr and target nuclei of ^{120}Sn and ^{109}Ag, with their intensities (without efficiency correction). For the ^{120}Sn target, values for three ranges of center-of-mass scattering angles used in the analysis are given.

Data set		I_i^π	I_f^π	E_γ (keV)	Counts	Error
35.9°–71.0°	^{96}Sr	2_1^+	0_1^+	815	167	15
	^{120}Sn	2_1^+	0_1^+	1171	20	7
71.0°–103.8°	^{96}Sr	2_1^+	0_1^+	815	240	30
	^{120}Sn	2_1^+	0_1^+	1171	45	7
103.8°–139.9°	^{96}Sr	2_1^+	0_1^+	815	280	30
		0_2^+	2_1^+	414	8	6
	^{120}Sn	2_1^+	0_1^+	1171	63	9
37.5°–139.9°	^{96}Sr	2_1^+	0_1^+	815	350	20
	^{109}Ag	$3/2^-$	$1/2^-$	311	1410	40
		$5/2^-$	$1/2^-$	415	1430	40

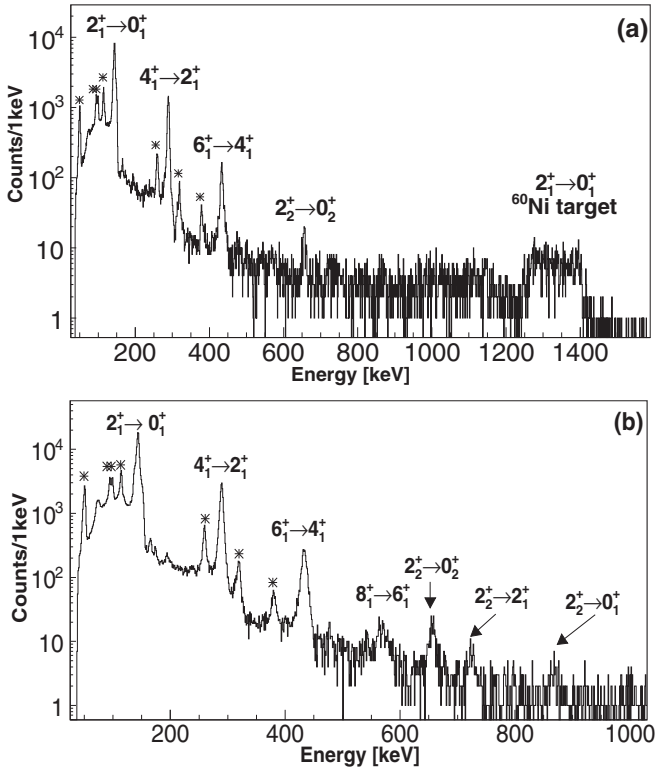

FIG. 3. (a) Total γ-ray spectrum from MINIBALL, following Coulomb excitation of the ^{98}Sr beam impinging on a ^{60}Ni target, Doppler corrected for the projectile. (b) Same spectrum for the excitation of ^{98}Sr on the ^{208}Pb target. The origin of the unknown transitions marked with asterisks is discussed in the text. Reproduced from Ref. [28].

ion has been stopped either in the silicon detector or in the target chamber, and consequently their energies appear shifted following the Doppler correction procedure. The ratio between the stopped (shifted) and in-flight (unshifted) component evolves as a function of the scattering angle, according to the lifetime of the state. This is due to the increase in the time of flight, related to a longer flight path, as well as to the velocity of ^{98}Sr ions decreasing with scattering angle. We applied the RDDS method [29] in order to extract the 2_1^+ lifetime from the intensities of the stopped and in-flight components, requesting relative angles between the scattered Sr ion and the emitted γ ray to fulfill the criterion $|\cos(\psi_{\mathrm{Proj}-\gamma})| \geqslant 0.5$, which assured good separation between the components. The spectra for three ranges of scattering angles, i.e., three distances between the target and the silicon detector, are presented in Fig. 4. The spectra are Doppler corrected for the projectile. The central peak, at the correct energy, corresponds to in-flight decay, while the two peaks at lower and higher energies correspond to the decay occuring at rest for backward and forward MINIBALL clusters, respectively. For clarity, the spectra are normalized to the intensity of the in-flight peaks. The blue spectrum corresponds to lower scattering angles, i.e. a shorter distance covered at higher velocity, and the green spectrum to higher scattering angles, i.e., a greater distance covered at lower velocity. A coherent evolution of the intensity ratio of the shifted and the unshifted component is clearly visible.

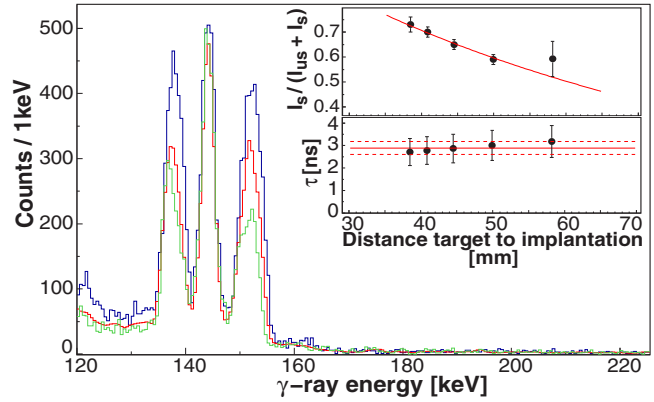

FIG. 4. Doppler corrected spectra for ^{98}Sr on ^{208}Pb, for three ranges of scattering angles (blue: 15°–22°; red: 23°–30°; green: 31°–39°, in the laboratory frame) zoomed in on the $2_1^+ \rightarrow 0_1^+$ decay in ^{98}Sr. In the inset the RDDS analysis for the 2_1^+ state is presented. Top: Standard decay function as a function of the target-to-DSSSD distance. I_s denotes the intensity of the shifted component, while I_{us} that of the unshifted one. Bottom: Deduced 2_1^+ lifetime for each distance and the global fit.

In the inset, a standard decay curve as a function of the distance is shown, as well as the 2_1^+ lifetime obtained using the differential decay curve method [29]. The extracted lifetime of $\tau = 2.9(3)$ ns is shorter than the literature value $\tau = 4.01(11)$ ns [27]. A possible reason for the disagreement is an important decrease of the MINIBALL efficiency for decays occurring after implantation in the silicon detector: as the number of counts in the stopped peak is underestimated, the deduced lifetime appears shorter. Due to this effect, which is difficult to quantify, some γ-ray intensities had to be excluded from the Coulomb excitation analysis as described in the following section.

As in the case of ^{96}Sr, the data for ^{98}Sr were divided into several subsets, corresponding to different ranges of scattering angles. The γ-ray intensities extracted for each data set are summarized in Table II, and the partial level scheme of ^{98}Sr, showing the observed transitions, is presented in Fig. 2. The $2_2^+ \rightarrow 0_1^+$ transition at 870 keV, although visible in the total spectrum, was too weak to be reliably fitted in the spectra corresponding to separate subranges of scattering angles.

B. ^{98}Rb

The spectra presented in Fig. 3 display unknown transitions at 50.2(3), 94.7(14), 99.1(13), 113.8(2), 258.4(2), 318.3(8), and 378.4(14) keV. The analysis of γ-γ coincidences shows that they are not in coincidence with any known transition in ^{98}Sr or in ^{98}Y. We therefore assume that these transitions belong to the beam contaminant ^{98}Rb, for which no excited states have been firmly established. This assumption is supported by the fact that similar low-energy γ rays, in mutual coincidence, were identified in neighboring nuclei: in ^{96}Rb, a cascade of 59.3- and 89.5-keV transitions, deexciting to the ground state, was established [30], while in the $N = 61$ isotone ^{100}Y the two lowest transitions in the band built on the 10.7-keV, 1^+ state have energies of 65.5 and 95.9 keV [31].

TABLE II. Intensities (without efficiency correction) of γ-ray transitions in ^{98}Sr following Coulomb excitation on ^{208}Pb and ^{60}Ni targets, for the ranges of center-of-mass scattering angles used in the analysis.

Data set	I_i^π	I_f^π	E_γ (keV)	Counts	Error
^{98}Sr + ^{208}Pb	2_1^+	0_1^+	144	38000	500
29.2°–41.9°	4_1^+	2_1^+	289	1410	50
	6_1^+	4_1^+	433	56	13
^{98}Sr + ^{208}Pb	2_1^+	0_1^+	144	38100	500
45.2°–68.1°	4_1^+	2_1^+	289	4680	80
	6_1^+	4_1^+	433	380	30
	2_2^+	0_2^+	655	47	9
^{98}Sr + ^{208}Pb	2_1^+	0_1^+	144	39870	1480
84.4°–127.3°	4_1^+	2_1^+	289	10820	140
	6_1^+	4_1^+	433	1910	50
	8_1^+	6_1^+	565	140	40
	2_2^+	2_1^+	727	42	13
	2_2^+	0_2^+	655	110	30
^{98}Sr + ^{208}Pb	2_1^+	0_1^+	144	4730	440
132.5°–139.9°	4_1^+	2_1^+	289	1390	60
	6_1^+	4_1^+	433	390	20
	8_1^+	6_1^+	565	45	10
	2_2^+	2_1^+	727	12	5
	2_2^+	0_2^+	655	29	7
^{98}Sr + ^{60}Ni	2_1^+	0_1^+	144	26700	900
54.0°–69.9°	4_1^+	2_1^+	289	2510	100
	6_1^+	4_1^+	433	200	20
	2_2^+	0_2^+	655	51	12
^{98}Sr + ^{60}Ni	2_1^+	0_1^+	144	17700	900
72.7°–97.5°	4_1^+	2_1^+	289	4140	80
	6_1^+	4_1^+	433	610	30
	2_2^+	0_2^+	655	60	10
^{98}Sr + ^{60}Ni	2_1^+	0_1^+	144	5700	500
100.0°–112.9°	4_1^+	2_1^+	289	1410	50
	6_1^+	4_1^+	433	250	30
	2_2^+	0_2^+	655	24	6

TABLE III. Intensities (without efficiency correction) of γ-ray transitions in ^{98}Rb following Coulomb excitation on ^{208}Pb and ^{60}Ni targets, as a function of center-of-mass scattering angle. All energies are given in keV.

Data set	E_γ (keV)	Counts	Error
^{98}Rb + ^{208}Pb	50.2	2790	180
29.2°–41.9°	94.7	520	120
	99.1	600	130
	113.8	2530	190
	258.4	550	40
	318.3	60	60
^{98}Rb + ^{208}Pb	50.2	2890	130
45.2°–68.1°	94.7	1440	150
	99.1	1570	130
	113.8	3050	300
	258.4	730	60
	318.3	170	30
	378.4	50	16
^{98}Rb + ^{208}Pb	50.2	3790	130
84.4°–127.3°	94.7	4130	140
	99.1	4330	180
	113.8	5000	500
	258.4	1200	200
	318.3	800	300
	378.4	210	80
^{98}Rb + ^{208}Pb	50.2	440	220
132.5°–139.9°	94.7	630	50
	99.1	640	60
	113.8	600	60
	258.4	180	20
	318.3	101	14
^{98}Rb + ^{60}Ni	50.2	2050	80
54.0°–69.9°	94.7	1110	110
	99.1	1050	120
	113.8	2500	150
	258.4	410	30
^{98}Rb + ^{60}Ni	50.2	1500	150
72.7°–97.5°	94.7	1580	120
	99.1	1550	120
	113.8	2090	110
	258.4	380	30
	318.3	210	20
	378.4	90	12
^{98}Rb + ^{60}Ni	50.2	450	60
100.0°–112.9°	94.7	560	40
	99.1	640	50
	113.8	640	40
	258.4	131	16
	318.3	81	11
	378.4	36	9

The measured intensities of γ-ray transitions in ^{98}Rb, Coulomb excited on ^{60}Ni and ^{208}Pb targets, are presented in Table III. The data were subdivided into several ranges of scattering angle in order to distinguish between single-step and multistep excitation processes and thus enable correct ordering of transitions observed in the γ-γ coincidence analysis. The proposed ^{98}Rb level scheme is presented in Fig. 5.

The transitions at 50.2, 94.7, and 99.1 keV are mutually in coincidence in our experiment, as well as the 113.8–318.3 keV and the 258.4–378.4 keV lines. Transitions at 51, 95, and 115 keV have been observed in a multinucleon transfer study, where a ^{98}Rb beam was used to bombard a ^{12}C target [32], and they were tentatively assigned to ^{98}Rb. Since the beam energy used in Ref. [32] was close to the Coulomb barrier, and inelastic scattering of ^{98}Rb was observed on a target much lighter than those used in the present work, the probability of multistep excitation was strongly reduced, and consequently the transitions observed in this experiment can only correspond to one- or two-step excitations from the ground state. One can conclude that the 50.2- and 94.7-keV transitions depopulate the first two excited states in a cascade, while the 99.1-keV transition corresponds to the decay of the third excited state in the same cascade, populated by multistep excitation with the heavier target. The same conclusion can be drawn for the 113.8- and 318.3-keV sequence. In addition, as explained in detail in Sec. IV, from the inconsistency between the γ-ray yields of the 433-keV $6_1^+ \rightarrow 4_1^+$ transition in ^{98}Sr, measured at

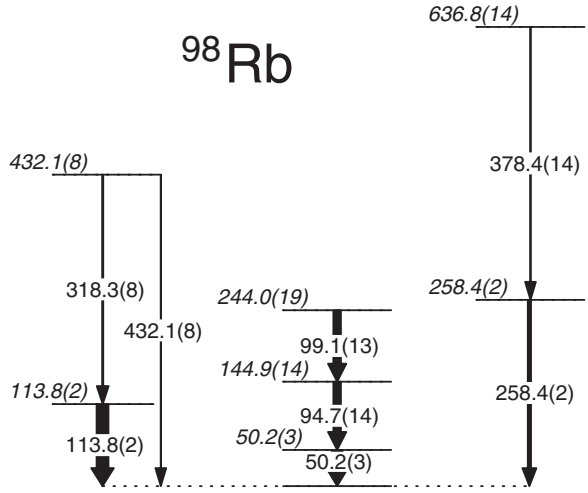

FIG. 5. Proposed level scheme of ^{98}Rb. Arrow widths reflect total intensities of transitions observed in the present experiment. Transition and level energies are given in keV.

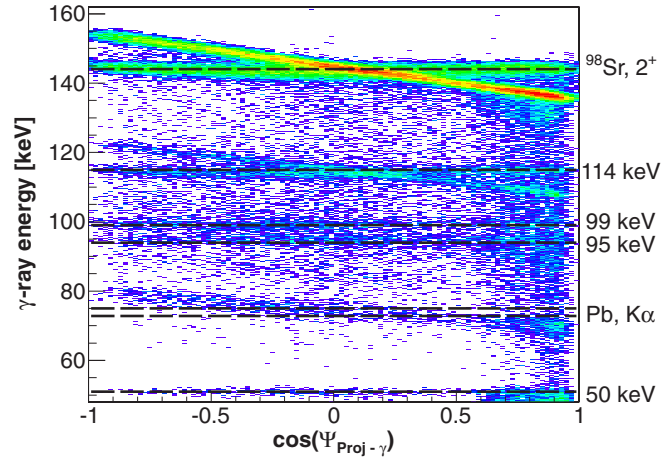

FIG. 6. Measured γ-ray energies, after Doppler correction for the velocity of ^{98}Rb /^{98}Sr nuclei, as a function of the cosine of the angle between the velocity vector of the scattered projectile and the direction of the γ-ray emission.

forward and backward scattering angles, we concluded that it overlapped with a line in ^{98}Rb of similar energy. We therefore propose a state in ^{98}Rb at 432.1 keV that decays either directly to the ground state, or via subsequent 318.3- and 113.8-keV transitions. We also note an enhancement of the 378.4-keV transition in coincidence with particles scattered at high CM angles, which suggests that this line corresponds to a decay of a state populated in multistep excitation. In contrast, the intensity of the 258.4-keV transition changes as a function of scattering angle in a way similar to that observed for the 113.8- and 50.2-keV transitions, hence we postulate a sequence of excited states in ^{98}Rb at 258.4 and 636.8 keV.

These observations can also be compared with the results obtained from the delayed γ-ray spectroscopy of fission fragments [33,34], where isomers with lifetimes ranging from a few hundreds of nanoseconds to a few microseconds were studied in mass-separated fission products.

In both experiments, 124- and 178-keV γ-ray transitions, correlated with detection of ^{98}Rb nuclei in the focal plane of the spectrometer, were interpreted as two decay paths of a 700-ns [33] or 358-ns [34] isomer at 178 keV, with the former feeding an intermediate state at 54 keV, which could not be observed due to the low detection efficiency at this energy. This intermediate state could be the 50.2(3)-keV level observed in the present experiment. In addition, a 116-keV transition was also observed in Ref. [33], possibly compatible with the 113.8(2)-keV line observed in the present work, but ruled out in Ref. [34]. It should be noted that the Coulomb excitation cross section for populating a long-lived isomeric state would be extremely low and it is, therefore, not surprising that the lines corresponding to the decay of the isomer were not observed in the present experiment.

Since the observed states in ^{98}Rb are populated in low-energy Coulomb excitation, they must be linked to the ground state by a sequence of $E2$ or $E3$ transitions, with possible admixtures of other multipolarities. In particular, all transitions linking the ground state and the proposed states at 113.8 and 432.1 keV should have an $E2$ component, otherwise it would not be possible to observe all three due to different timescales for $E1$, $E2$, and $E3$ decays. This implies the same parity for the states at 113.8 and 432.1 keV and for the ground state, and if the spin of the ground state is equal to zero [27,35] it leads to the assignment of spin 2 for the state at 113.8 keV, and either 1 or 2 spin assignment for the 432.1-keV state.

Estimates of some of the lifetimes of excited states in ^{98}Rb can be made using the effect demonstrated in Fig. 4: if the time of flight between the target and the silicon strip detector is comparable to the lifetime of the given state, the corresponding γ-ray line will exhibit extra peaks on both sides, as observed for the 144-keV transition in ^{98}Sr. Figure 6 shows measured γ-ray energies, after Doppler correction for the velocity of ^{98}Rb /^{98}Sr nuclei, as a function of the cosine of the angle between the velocity vector of the scattered projectile and the direction of the γ-ray emission. Three different patterns are observed. First, for the 144-keV transition in ^{98}Sr and the 114-keV line in ^{98}Rb some γ rays are properly Doppler corrected and appear at the correct energy for all combinations of angles (horizontal lines in Fig. 6), while others correspond to the decay at rest and appear as diagonal lines on the plot. For these two transitions it is clear that the corresponding lifetimes are comparable to the time of flight between the target and the particle detector. Second, the 50.2-, 94.7-, and 99.1-keV lines in ^{98}Rb are properly corrected for the Doppler effect for all combinations of angles, which means that the decay takes place in flight. Finally, Pb x rays appear wrongly Doppler corrected, since the kinematics of the projectile was assumed in the Doppler correction procedure.

An RDDS analysis, similar to that carried out for the 2^+ state in ^{98}Sr, which was presented in Sec. III A, can be performed for the 114-keV state in ^{98}Rb. Such an approach yields a mean lifetime of $\tau = 1.2(3)$ ns, but it clearly suffers from a similar problem of reduction of the MINIBALL efficiency for the decays taking place at rest, as observed for the 2^+ state in ^{98}Sr. A proper estimate of this correction factor would require

knowledge of the multipolarity of the 114-keV transition, which influences particle-γ correlations and thus the measured γ-ray intensities. As a first approximation, we propose to simply scale the obtained mean lifetime by a factor of 1.4, which corresponds to the difference between the literature value of the 2_1^+ lifetime in ^{98}Sr [4.01(11) ns] and that obtained in the present RDDS analysis [2.9(3) ns]. This yields a value of $\tau = 1.7(5)$ ns, which, assuming a pure electric quadrupole character for the 114-keV transition, would correspond to a transition probability exceeding 500 Weisskopf units. Hence, we conclude that the 114-keV transition must have a significant $M1$ admixture. This, however, would exclude a 0^+ spin-parity for the ground state, since the selection rules do not permit a mixed $E2/M1$ transition decaying to a 0^+ state. The only possibilities would be transitions of pure $M1$ or pure $E2$ character. The former is inconsistent with the population of the 113.8-keV state in one-step Coulomb excitation observed in the work of Bottoni *et al.* [32], and the latter with the obtained lifetime.

Finally, from the fact that the 50.2-, 94.7-, and 99.1-keV transitions can be properly Doppler corrected, we can estimate that the mean lifetimes of the 50.2-, 114.9-, and 224-keV levels in ^{98}Rb are shorter than 1 ns. For comparison, the lifetime of the second state in a similar cascade in $N = 61$ isotone ^{100}Y is equal to 72(8) ps [36].

IV. COULOMB EXCITATION ANALYSIS

The Coulomb excitation analysis was performed using the least-squares fitting code GOSIA and its version capable of handling the mutual excitation of collision partners, GOSIA2 [37–39]. Both versions of the code use a standard χ^2 function constructed from the measured γ-ray yields and those calculated from a set of electromagnetic matrix elements, both transitional and diagonal, between all states involved in the excitation process. Known spectroscopic data, such as lifetimes, mixing and branching ratios, can be used as additional data points in the minimization procedure.

For ^{96}Sr, where prior to the present experiment the lifetime of the first 2^+ was known with a large uncertainty (7(4) ps [10]), normalization of measured γ-ray intensities to the target excitation was necessary. The GOSIA2 code was used to find a set of matrix elements that optimally reproduced the γ-ray yields listed in Table I for both target and projectile excitation. The lifetime of the excited 0^+ state [10] was included in the minimization, as well as transitional and diagonal matrix elements for the ^{120}Sn and the ^{109}Ag target nuclei [27]. The statistics collected using the ^{120}Sn target were sufficient to subdivide the data into three angular ranges and, in this way, to study the influence of the quadrupole moment of the 2_1^+ state on its excitation cross section via the reorientation effect. Only the 2_1^+ and 0_2^+ excited states were included in the minimization process; due to the high excitation energy of the 4_1^+ state, it does not affect the population of lower-lying states in the Coulomb excitation process. As the statistics obtained for the $0_2^+ \rightarrow 2_1^+$ transition were low, the influence of the two-step excitation of the 0_2^+ level on the excitation probability of the 2_1^+ state, competing with the reorientation effect, was further constrained by including the known lifetime of this level [10] in the minimization procedure. The $E0$ decay of the 0_2^+ state in ^{96}Sr was not considered in the GOSIA analysis, since in electron spectroscopy measurements that yielded a very strong electric monopole transition between the 0_3^+ and the 0_2^+ states [11–13] no $E0$ transition from any of the excited 0^+ states to the ground state was observed. Since only two transitional matrix elements are needed to describe the observed excitation, interference effects are not present and thus only absolute values of these matrix elements could be determined.

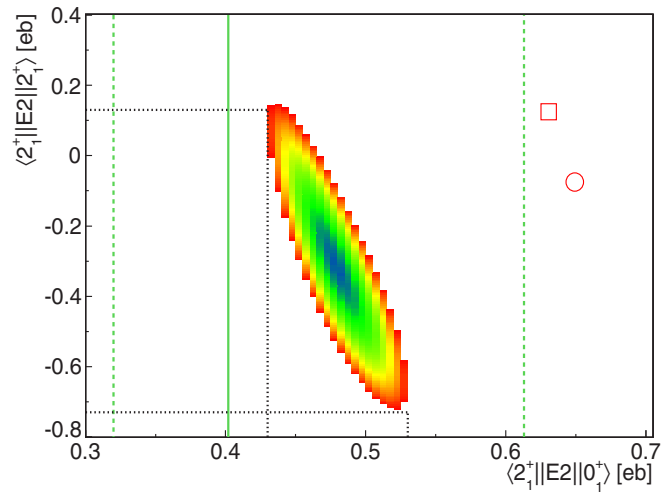

FIG. 7. A two-dimensional χ^2 surface with respect to $\langle 2_1^+ \| E2 \| 0_1^+ \rangle$ and $\langle 2_1^+ \| E2 \| 2_1^+ \rangle$ in ^{96}Sr, obtained for Coulomb excitation of ^{96}Sr on ^{120}Sn. A 1σ cut is applied with the condition that $\chi^2 < \chi^2_{\min} + 1$. The vertical green lines correspond to the previously reported value of the 2_1^+ lifetime (solid) and its uncertainty (dashed). The black dotted lines illustrate how the uncertainties of matrix elements were determined. The red open square and the circle represent the results of theoretical calculations using the complex excited VAMPIR approach [40] and beyond-mean-field calculations with the Gogny D1S interaction, respectively (see Sec. V).

Figure 7 presents the χ^2 surface resulting from the comparison of the measured and calculated γ-ray intensities in ^{96}Sr and ^{120}Sn, as well as the spectroscopic data mentioned above, with respect to the $\langle 2_1^+ \| E2 \| 0_1^+ \rangle$ and $\langle 2_1^+ \| E2 \| 2_1^+ \rangle$ matrix elements in ^{96}Sr. The uncertainties of the target matrix elements and the statistical errors of the γ ray intensities are taken into account in the calculation of the χ^2 function. A minimum χ^2 value of 1.15 was found for a combination of matrix elements presented in Table IV. Following the prescription described in Ref. [39], the 1σ uncertainties of both matrix elements were obtained by projecting the contour corresponding to $\chi^2_{\min} + 1$ on their respective axes, as illustrated by the black dotted lines in Fig. 7. The green vertical lines in Fig. 7 correspond to the mean value and related error bars for the $\langle 2_1^+ \| E2 \| 0_1^+ \rangle$ matrix element, deduced from the earlier measurement of the 2_1^+ lifetime [10]. The transitional matrix element is in perfect agreement with the value calculated from the previously reported lifetime, and its precision is significantly improved. The diagonal matrix element is found to be negative and small, which can be interpreted as an indication of a weakly deformed prolate shape.

TABLE IV. Transitional and diagonal $E2$ and $M1$ matrix elements in ^{96,98}Sr.

I_1^π	I_2^π	^{98}Sr $\langle I_2\|E2\|I_1\rangle$ (eb)	^{96}Sr
2_1^+	0_1^+	$1.13^{+0.01}_{-0.01}$	$0.47^{+0.05}_{-0.04}$
4_1^+	2_1^+	$1.76^{+0.05}_{-0.05}$	
6_1^+	4_1^+	$2.46^{+0.11}_{-0.10}$	
8_1^+	6_1^+	$2.37^{+0.17}_{-0.14}$	
2_2^+	0_2^+	$0.41^{+0.03}_{-0.03}$	
2_2^+	0_1^+	$-0.101^{+0.008}_{-0.008}$	
0_2^+	2_1^+	$0.404^{+0.014}_{-0.017}$	
2_2^+	2_1^+	$\|0.07^{+0.10}_{-0.05}\|$	
2_2^+	4_1^+	$0.23^{+0.09}_{-0.08}$	
2_1^+	2_1^+	$-0.63^{+0.32}_{-0.28}$	$-0.30^{+0.45}_{-0.41}$
4_1^+	4_1^+	$-2.82^{+0.21}_{-0.22}$	
6_1^+	6_1^+	$-1.86^{+0.33}_{-0.31}$	
8_1^+	8_1^+	$-1.40^{+1.50}_{-1.29}$	
2_2^+	2_2^+	$+0.04^{+0.32}_{-0.20}$	
I_1^π	I_2^π	$\langle I_2\|M1\|I_1\rangle$ (μ_N)	
2_2^+	2_1^+	$\|0.09^{+0.01}_{-0.02}\|$	

Due to a lower level of statistics and the inability to distinguish between ^{96}Sr and ^{109}Ag particles detected in the DSSSD, a similar analysis of the data collected with the ^{109}Ag target could not be performed. From a single angular range it is impossible to determine both the transitional and diagonal matrix elements without additional constraints. However, the transitional matrix element extracted from this data set, assuming $\langle 2_1^+\|E2\|2_1^+\rangle$ within the rotational limits, has been found to be consistent within 1σ with the result obtained using the ^{120}Sn target.

For ^{98}Sr, the known lifetimes of the 2_1^+, 4_1^+, 8_1^+, 10_1^+, and 0_2^+ states [10,14–19] (see Table V) and the branching ratios for the 0_2^+ and 2_2^+ decays [17,20,21,27] were used as additional data points in the GOSIA fit.

The $(0_2^+ \rightarrow 2_1^+)/(0_2^+ \rightarrow 0_1^+)$ branching ratio, measured in electron spectroscopy following the β decay of ^{98}Rb [20,21], was also included in the analysis. Since it is not currently possible to introduce data related to $E0$ decay directly into the GOSIA input files, an indirect method was utilized. In addition to the known level scheme of ^{98}Sr, an extra level of spin and parity 1^+ was declared below the 2_1^+ state, at 130 keV

TABLE V. Lifetimes in ^{98}Sr known from earlier measurements, used in the present Coulomb excitation analysis as additional data points, and those resulting from the GOSIA fit.

I^π	τ (ps)	τ (ps) (GOSIA)
2_1^+	$4.01(11) \times 10^3$ [14]	$4.00(8) \times 10^3$
4_1^+	115.4(86) [14]	113.8(29)
6_1^+		11.34(08)
8_1^+	4.32(72) [18]	4.24(51)
0_2^+	$32.8(2) \times 10^3$ [17,20]	$33(11) \times 10^3$
2_2^+		12.4(20)

excitation energy, and connected to the 0_2^+ state by a 85-keV $M1$ transition. Since population of excited states in ^{98}Sr proceeds almost exclusively via $E2$ transitions, introduction of such an additional state does not affect the calculated excitation pattern. The $\langle 1^+\|M1\|0_2^+\rangle$ matrix element has been fitted in such a way that the intensity of the $0_2^+ \rightarrow 1^+$ transition, normalized to that of $0_2^+ \rightarrow 2_1^+$, $\mathcal{R}$, reproduces the $E0/E2$ branching ratio measured in electron spectroscopy [20,21], R, corrected for internal conversion as follows:

$$\mathcal{R} = \frac{I_\gamma(0_2^+ \rightarrow 1^+)}{I_\gamma(0_2^+ \rightarrow 2_1^+)} = R(E0/E2) \times \frac{1+\alpha_{E2,71\,\mathrm{keV}}}{1+\alpha_{M1,85\,\mathrm{keV}}}. \quad (1)$$

In this way, an alternative decay path of the 0_2^+ state has been included in the calculation, which does not modify the direct population of excited states in the Coulomb excitation process. It is worth noting that the partial lifetime for the virtual $M1$ decay corresponds to that for the $E0$ decay, and consequently the experimental value of the total 0_2^+ lifetime can be used as a constraint in the Coulomb excitation procedure without need for any corrections. This procedure has been tested and validated in Refs. [41–43]. In particular, in Ref. [43] the $E0$ component of the $2_2^+ \rightarrow 2_1^+$ transition was taken into account in addition to the $0_2^+ \rightarrow 0_1^+$ decay. In this case, it has been additionally verified that changing the multipolarity of the virtual transition simulating the $E0$ branch from $M1$ to $M2$ does not affect the final values of matrix elements. This shows that the multipolarity of the feeding transition affects the population of magnetic substates in a way that has a negligible influence on calculated γ-ray intensities, at least in comparison with experimental uncertainties of measured γ-ray yields. This effect may only play a role when the $E0$ decay feeds an excited state, and not for $E0$ transitions decaying directly to the ground state. For ^{98}Sr, we assumed that the $2_2^+ \rightarrow 2_1^+$ has an $E2/M1$ character without any $E0$ admixture, as in earlier electron spectroscopy studies [12,20,21] no electron peak was observed corresponding to the decay of the 2_2^+ state at 871 keV.

Data collected using the ^{60}Ni and ^{208}Pb targets were fitted simultaneously in order to enhance sensitivity to higher-order effects, such as quadrupole moments and relative signs of electromagnetic matrix elements. In total, 17 matrix elements were fitted to 31 data points. Although the $2_2^+ \rightarrow 4_1^+$ transition was too weak to be directly observed, the corresponding matrix element could be determined from the measured γ-ray intensities as a function of the scattering angle and atomic number of the target, combined with known branching ratios, as it affected excitation cross sections of observed states, in particular those of the 2_2^+ and 4_1^+ states. For the $2_2^+ \rightarrow 0_1^+$ transition, 29(7) counts were observed using the ^{208}Pb target, in coincidence with particles scattered in the 45.2°–139.9° CM angular range (experiments 2–4 in Table II). This intensity was included in the GOSIA fit, together with that of the $4_1^+ \rightarrow 2_1^+$ transition measured for the same angular range, which ensured proper normalization [39]. However, as the uncertainty of the $(2_2^+ \rightarrow 0_1^+)/(2_2^+ \rightarrow 0_2^+)$ branching ratio (16%) is significantly lower than that of the $2_2^+ \rightarrow 0_1^+$ intensity (24%), it is not surprising that including this intensity in the minimisation process did not affect the final set of fitted matrix elements, nor their uncertainties.

The signs of all in-band transitional matrix elements were chosen to be positive, as well as that of $\langle 2_1^+ \| E2 \| 0_2^+ \rangle$. The signs of remaining transitional matrix elements were determined relative to those. Changing the sign of the $\langle 2_2^+ \| E2 \| 0_1^+ \rangle$ matrix element resulted in tenfold increase of the χ^2 value, while a sixfold effect was observed when the sign of $\langle 4_1^+ \| E2 \| 2_2^+ \rangle$ was changed. No sensitivity to the signs of the $\langle 2_2^+ \| E2 \| 2_1^+ \rangle$ and $\langle 2_2^+ \| M1 \| 2_1^+ \rangle$ matrix elements was observed.

As mentioned in Sec. III, due to the long lifetime of the 2_1^+ state, the $2_1^+ \rightarrow 0_1^+$ γ-ray yield was affected by the reduction of the MINIBALL efficiency for decays taking place far from the target. The measured yields for this transition were found to be in disagreement with what would be expected assuming the known lifetime of the 2_1^+ state. The disagreement was most important for low center-of-mass (CM) angles: experimental $2_1^+ \rightarrow 0_1^+$ yields were too low by a factor of 2.1 and 1.5 for the first and the second angular range, respectively, for the ^{208}Pb target and by a factor 1.7 for the first set collected with the ^{60}Ni target (Table II). For the remaining angular ranges, the measured $2_1^+ \rightarrow 0_1^+$ γ-ray intensities could be reproduced within 1σ. The range of scattering angles, where the calculated and measured yields disagree, corresponds to the direct scattering of ^{98}Sr into the DSSSD, with a velocity that assures that a substantial fraction of the decay occurs at rest. This effect is fully consistent with the conclusion drawn from the RDDS analysis. As a consequence, the $2_1^+ \rightarrow 0_1^+$ yields were included in the minimisation procedure only for the two data sets for each target that corresponded to the highest CM angles.

Another transition, for which a systematic disagreement was observed for lower CM angles, was the $6_1^+ \rightarrow 4_1^+$ decay at 433.2 keV. The energy of this transition is very close to the sum of the $2_1^+ \rightarrow 0_1^+$ and $4_1^+ \rightarrow 2_1^+$ energies (144.2 and 289.3 keV, respectively). The contribution arising from summing of these two transitions within a single MINIBALL cluster during the add-back procedure was deduced from the γ-γ matrix, constructed within a single cluster, to be below 3% of the 433.2-keV line intensity, which cannot explain the magnitude of the observed effect nor the fact that it changes as a function of particle scattering angle. Another possible reason for this disagreement could be an overlap with a transition in a beam contaminant. As described in Sec. III B, two mutually coincident transitions of 113.8(2) keV and 318.3(8) keV energy have been observed in the spectra and assigned to ^{98}Rb. A state at 432.1 keV is, therefore, proposed that decays either directly to the ground state via a 432.1-keV γ ray or by a cascade of two transitions at 113.8(2) and 318.3(8) keV. The Coulomb excitation analysis further supports this assumption as the disagreement is observed only at low CM angles, where three-step excitation to the 6^+ state in ^{98}Sr would be less favored than one- or two-step excitation of the hypothetical 432.1-keV state in ^{98}Rb. As the magnitude of this effect is difficult to estimate, the $6_1^+ \rightarrow 4_1^+$ transition intensities measured for the first two datasets for each target were excluded from the minimisation process. In addition, a systematic error of 3%, arising from the add-back procedure, was added to statistical uncertainties for the $6_1^+ \rightarrow 4_1^+$ transition for the remaining data sets.

The calculation of γ-ray yields within the GOSIA code includes effects influencing γ-ray intensities, such as internal conversion, the finite size and relative efficiency of Ge detectors, and the attenuation caused by the deorientation effect during recoil in vacuum. Conversion coefficients for the observed transitions were calculated using the BRICC calculator [44] except for the 50 keV $0_2^+ \rightarrow 2_1^+$ transition lying below the K edge, where the measured ICC value [45] was used. Influence of the g factor of the 2_1^+ state in ^{98}Sr on measured γ-ray yields due to deorientation effect was also investigated. Since this g factor has not been measured, the approximation $g = Z/A$ was initially used in the GOSIA calculations. However, a recent measurement for ^{82,90}Sr has shown that the g factors in Sr nuclei behave identically as a function of the neutron number to those in the Zr isotopes [46], thus the g factor in ^{98}Sr should be close to the value of $+0.30(3)$ measured for ^{100}Zr [47]. γ-ray intensities calculated using the standard $g = \mathrm{Z}/A = 0.38\mu_N$ value and those assuming $g = 0.30\mu_N$ agree within error bars, and consequently this change has no effect on extracted matrix elements.

As a result of the minimization process, a set of matrix elements was found that allows for the reproduction of all experimental γ-ray yields as well as other spectroscopic data within 1σ. The obtained transitional and diagonal electromagnetic matrix elements are presented in Table IV. Lifetimes of the 6_1^+ and 2_2^+ states have been determined for the first time, while the precision of those for the 4_1^+ and 8_1^+ states was improved, as presented in Table V. From the obtained $E2$ and $M1$ matrix elements, a $\delta(E2/M1)$ mixing ratio equal to 0.7(10) can be extracted for the $2_2^+ \rightarrow 2_1^+$ transition.

It should be noted that the errors presented in Tables IV and V are statistical only, and in particular that the error for the $2_1^+ \rightarrow 0_1^+$ transition in ^{98}Sr reflects the precision of the earlier lifetime measurement. The systematic error of matrix elements extracted from Coulomb excitation data, resulting from approximations used in the GOSIA code, is estimated to be smaller than 3% [38,39].

V. DISCUSSION

The measured spectroscopic quadrupole moments and transition probabilities confirm the shape coexistence scenario and the shape change from a nearly spherical ground state in ^{96}Sr to a high-deformed ground-state band in ^{98}Sr [22,23].

The matrix elements have been further analyzed using the quadrupole sum rules approach [25,48]. This method relates experimentally determined $E2$ matrix elements to deformation parameters, defined in the intrinsic frame of the nucleus, by constructing quadrupole invariants $\langle \mathcal{Q}^2 \rangle$ and $\langle \mathcal{Q}^3 \cos(3\delta) \rangle$. The $\mathcal{Q}$ parameter describes the magnitude of the deformation, while the δ parameter measures triaxiality. In order to determine the $\langle \mathcal{Q}^2 \rangle$ invariant for a 0^+ state, one has to measure absolute values of all $E2$ matrix elements that couple the state in question with low-lying 2^+ states. To obtain the triaxiality parameter, $\langle \cos(3\delta) \rangle$, more experimental information is needed, namely transitional matrix elements, together with their relative signs, between the state in question and 2^+ states, those coupling the 2^+ states one to another, as well as diagonal $E2$ matrix elements of the 2^+ states.

The results for ^{96}Sr and ^{98}Sr are presented in Fig. 8. For the ^{96}Sr case, the matrix elements connecting the 0_1^+

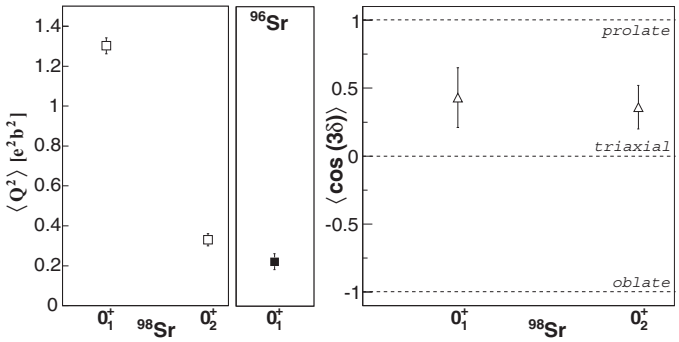

FIG. 8. Quadrupole deformation parameters obtained with the sum-rule method for the $0^+_{1,2}$ states in ^{98}Sr and 0^+_1 in ^{96}Sr.

to the $2^+_{2,3}$ states at 1506 and 1628 keV, respectively, are unknown. In principle, the quadrupole invariants $\langle\mathcal{Q}^2\rangle$ and $\langle\mathcal{Q}^3\cos(3\delta)\rangle$ for the ground state in ^{96}Sr cannot be deduced from our measurement. However, as shown in Ref. [48], the $\langle\mathcal{Q}^2\rangle$ invariant for the ground state in even-even nuclei is dominated by the contribution of the $\langle 0^+_1\|E2\|2^+_1\rangle$ matrix element. In particular, it was shown in a recent study of the neighboring $N = 58$ nucleus ^{100}Mo [42] that the $\langle 0^+_1\|E2\|2^+_2\rangle$ and $\langle 0^+_1\|E2\|2^+_3\rangle$ matrix elements contribute less than 2% to the final $\mathcal{Q}^2$ value for the ground state. Assuming a similar scenario for ^{96}Sr, a $\langle\mathcal{Q}^2\rangle$ value equal to 0.22(4) e^2b^2 can be deduced from our measurement, corresponding to a rather low quadrupole deformation in agreement with the spectroscopic moment of the 2^+_1 state. The situation is more complex for the higher-order quadrupole invariant $\langle\mathcal{Q}^3\cos(3\delta)\rangle$. Again, for a 0^+ ground state only limited information is required, compared to higher-lying states. Reference [49] demonstrates that this invariant can be derived with good accuracy using only four matrix elements: $\langle 0^+_1\|E2\|2^+_1\rangle$, $\langle 2^+_1\|E2\|2^+_1\rangle$, $\langle 2^+_1\|E2\|2^+_2\rangle$, and $\langle 2^+_2\|E2\|0^+_1\rangle$. This is again confirmed by the results on ^{100}Mo [42], where other matrix elements amounted to less than 10% of the calculated $\langle\cos(3\delta)\rangle$ value. However, the contributions of $\langle 0^+_1\|E2\|2^+_1\rangle\langle 2^+_1\|E2\|2^+_1\rangle\langle 2^+_1\|E2\|0^+_1\rangle$ and $\langle 0^+_1\|E2\|2^+_1\rangle\langle 2^+_1\|E2\|2^+_2\rangle\langle 2^+_2\|E2\|0^+_1\rangle$ products were similar in magnitude. Since the $\langle 2^+_1\|E2\|2^+_2\rangle$ and $\langle 2^+_2\|E2\|0^+_1\rangle$ matrix elements in ^{96}Sr are not known, we cannot report any $\langle\cos(3\delta)\rangle$ value for the ground state in this nucleus.

In ^{98}Sr, an abrupt change in deformation is observed between the ground state [$\langle\mathcal{Q}^2\rangle = 1.30(4)$ e^2b^2] and the low-lying 0^+_2 state [$\langle\mathcal{Q}^2\rangle = 0.33(3)$ e^2b^2] consistent with the spectroscopic quadrupole moments measured for the $2^+_{1,2}$ states. One can observe that the deformation of the ground state in ^{96}Sr and that of the low-lying 0^+_2 state in ^{98}Sr are similar, supporting the scenario in which these two configurations interchange at $N = 60$. The triaxiality parameters $\langle\cos(3\delta)\rangle$ for both 0^+_1 and 0^+_2 states in ^{98}Sr, extracted from the present data, suggest a non-axially symmetric prolate shape, with the deformation parameter $\gamma \simeq (1/3)\arccos\langle\cos(3\delta)\rangle$ equal to 21° and 23° respectively. In view of the similarity between the 0^+_2 state in ^{98}Sr and the 0^+_1 state in ^{96}Sr, one might also expect significant triaxiality for the ground state in ^{96}Sr, which is consistent with the low negative value of the 2^+_1 spectroscopic quadrupole moment. However, more information on the $2^+_{2,3}$ states is clearly required to firmly establish the role of triaxiality in ^{96}Sr.

TABLE VI. Mixing amplitudes for the 0^+ and 2^+ states, intrinsic quadrupole moments for the two pure configurations (prolate and spherical), and diagonal $E2$ matrix elements of the unperturbed 2^+ states determined using the two-level mixing model.

$\cos^2\theta_0$	0.87(1)
$\cos^2\theta_2$	0.99(1)
Q_0^{pr}	+3.85(6) eb
$Q_0^{\rm sph}$	−0.5(3) eb
$\langle 2^+_p\|E2\|2^+_p\rangle$	−1.45(2) eb
$\langle 2^+_s\|E2\|2^+_s\rangle$	+0.18(10) eb

Triaxiality is often associated with the mixing of wave functions, hence we attempt to interpret the measured reduced matrix elements in ^{98}Sr using a simple two-state mixing model. In this model, the observed physical states $|I^+_1\rangle$ and $|I^+_2\rangle$ may be expressed as linear combinations of pure prolate and spherical configurations, $|I^+_p\rangle$ and $|I^+_s\rangle$ respectively:

$$|I^+_1\rangle = +\cos\theta_I \times |I^+_p\rangle + \sin\theta_I \times |I^+_s\rangle, \quad (2)$$

$$|I^+_2\rangle = -\sin\theta_I \times |I^+_p\rangle + \cos\theta_I \times |I^+_s\rangle. \quad (3)$$

Experimental data, in particular $E2$ matrix elements, can then be used to calculate the mixing amplitudes, $\cos^2\theta_I$, between the two pure (unperturbed) configurations. Such a model has been applied to ^{98}Sr in the past, but with less detailed experimental data. Schussler *et al.* [20], using the measured lifetime of the 2^+_1 and 0^+_2 states and the axial rotor model, extracted mixing amplitudes $\cos^2\theta_0 = 0.90$ and $\cos^2\theta_2 = 0.99$ for the 0^+_1 and 2^+_1 states, which suggest a very low degree of mixing between the two configurations. Similar conclusions have been obtained in Refs. [14,50]. More recently, Park *et al.* [21] deduced $\cos^2\theta_0 = 0.91$ and $\cos^2\theta_2 = 0.98$ from the new measurement of ^{98}Rb β decay combined with a systematic study of neighboring Kr, Zr, and Mo isotopes. Following the method described in our previous work [41], we have extracted from the complete set of $E2$ matrix elements the mixing angles for the 0^+ and 2^+ states wave functions [22,23], which are presented in Table VI. This model also yields intrinsic (unperturbed) intraband $E2$ matrix elements that can be converted to unperturbed transitional quadrupole moments Q_0. From those, under the assumption of the rotational model, one can calculate diagonal $E2$ matrix elements for the pure intrinsic configurations. The resulting values are presented in Table VI.

The transitional quadrupole moment Q^t_0 can be calculated from measured $E2$ matrix elements using the following formula:

$$eQ^t_0 = \sqrt{\frac{16\pi}{5}}\frac{1}{\sqrt{2I_1+1}}\frac{\langle I_2||\mathcal{M}(E2)||I_1\rangle}{\langle I_1K_120|I_2K_2\rangle}. \quad (4)$$

The obtained transitional quadrupole moment of the prolate state, Q^{pr}_0, equal to 3.85(6) eb, can be compared to those calculated from the measured transitional matrix elements

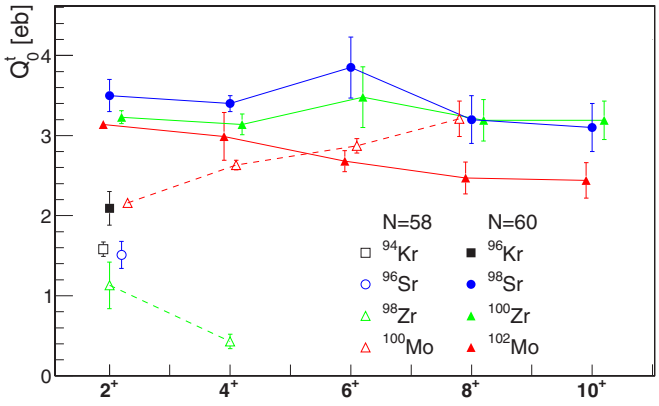

FIG. 9. Transitional quadrupole moments Q_0^t calculated from the $B(E2; J \rightarrow J-2)$ values in the ground-state band for Mo, Zr, Sr, and Kr $N = 58$ and $N = 60$ isotones. Some of the values are slightly displaced on the x axis for clarity.

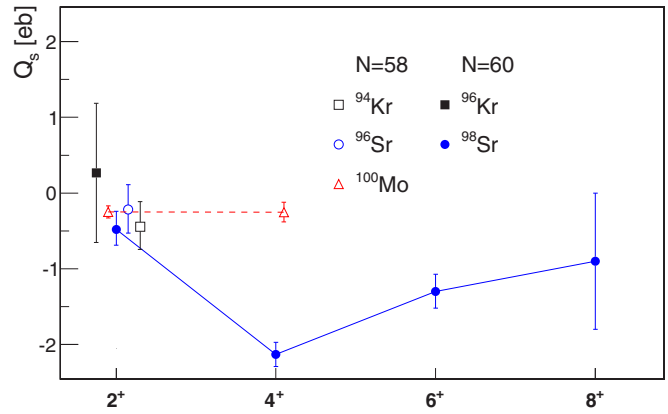

FIG. 10. Spectroscopic quadrupole moments Q_s calculated from diagonal $E2$ matrix elements measured for Mo, Sr, and Kr isotopes. Some of the values are slightly displaced on the x axis for clarity.

in the ground-state band: $Q_0^t = 3.5(2)$ eb, 3.4(1) eb, and 3.8(6) eb for the $2^+ \rightarrow 0^+$, $4^+ \rightarrow 2^+$, and $6^+ \rightarrow 4^+$ transitions, respectively. The agreement is good, and improves with increasing spin, as one would expect for a rotational band exhibiting weak mixing at low spin. On the other hand, the diagonal matrix element $\langle 2_p^+ \| E2 \| 2_p^+ \rangle$ for the pure prolate configuration, equal to $-1.45(2)e$b, is much higher than the experimental value for the the 2_1^+ state ($-0.63^{+0.32}_{-0.28}$ eb). This disagreement shows the limitations of the two-state mixing model. A possible reason for the observed reduction of the diagonal matrix element $\langle 2_1^+ \| E2 \| 2_1^+ \rangle$, as compared to the value obtained for the unperturbed prolate configuration, could be a certain amount of triaxiality, which is suggested by the results of the sum-rules analysis.

The transitional quadrupole moment for the second pure configuration, as well as the deduced diagonal matrix element $\langle 2_s^+ \| E2 \| 2_s^+ \rangle$, correspond to a much lower quadrupole deformation than that of the prolate configuration, in a qualitative agreement with the measured values of the $\langle 0_2^+ \| E2 \| 2_2^+ \rangle$ and $\langle 2_2^+ \| E2 \| 2_2^+ \rangle$ matrix elements. A quantitative comparison of $Q_0^{\rm sph}$ with the transitional quadrupole moments in the high-spin part of the band built on the 0_2^+, which are expected to be non-perturbed by the mixing, is unfortunately not possible as it is not clear how this band develops beyond the 2_2^+ state.

The systematics of transitional quadrupole moments Q_0^t in the ground-state band, as a function of spin, for the Mo, Zr, Sr, and Kr isotones with $N = 58$ and $N = 60$ is presented in Fig. 9. It includes the results obtained in the present work for ^{96,98}Sr, as well as preliminary results for 2_1^+ in ^{98}Zr [51] and 6_1^+ in ^{102}Mo [52]. The Q_0^t values in $N = 60$ ^{100}Zr and ^{98}Sr are large [an average value of $\langle Q_0^t \rangle = 3.38(8)$ eb], similar in magnitude for both nuclei and rather constant for all states, as expected for a rotational band. Both Mo isotopes, while exhibiting deformation similar to those of ^{100}Zr and ^{98}Sr, present systematic changes of Q_0^t as a function of spin. The Q_0^t moment in ^{100}Mo increases with spin; it has been established, however, that ^{100}Mo possesses a significant contribution of the triaxial degree of freedom at low excitation energy, which could reduce the Q_0^t value at low spins [42]. An inverse trend is observed for ^{102}Mo, interpreted as a rotational-to-vibrational transition at high spin. On the other hand, transitional quadrupole moments for the $N = 58$ isotones are considerably lower: the values for the 2_1^+ state in ^{96}Sr and ^{94}Kr are close to 1.5 eb, and those for ^{98}Zr are lower still. Finally, the Q_0^t value for the 2_1^+ state in ^{96}Kr significantly deviates from what is observed for the heavier $N = 60$ isotones and is comparable to the values obtained for the $N = 58$ ^{96}Sr and ^{94}Kr nuclei, confirming that the Kr isotopes lie outside the region of this shape change.

The systematics of experimentally determined spectroscopic quadrupole moments in the ground state bands of $N = 58$ and $N = 60$ Kr, Sr, and Mo nuclei, as a function of spin, is presented in Fig. 10. These results were obtained in safe Coulomb excitation experiments of ^{100}Mo [42] and ^{94,96}Kr [4] or determined in the present work. The results for the first 2^+ states in all nuclei are consistently low. The present data for ^{98}Sr show a sudden increase of the spectroscopic quadrupole moment at $J^\pi \geqslant 4^+$ that stabilises for higher spins, with an average value $\langle Q_s \rangle = -1.6(3)$ eb corresponding to an axial deformation $\beta_2 = +0.5(1)$. Such a large quadrupole deformation is not observed for $N = 58$ ^{100}Mo, where the quadrupole moment of the 4_1^+ state remains similar to that of the first excited state. In the shape coexistence framework, the increase in Q_s beyond the 2_1^+ state can be associated with the mixing of the 2^+ wave functions that reduces the spectroscopic quadrupole moment of the 2_1^+ state. However, the two-state mixing model analysis indicates weak mixing. Hence, we tentatively attribute the observed reduction of the Q_s of the 2_1^+ state to a certain level of triaxiality at low excitation energy. In order to estimate the γ deformation needed to explain the experimental value of the Q_s, we studied the dependence of the $\langle 2_1^+ \| E2 \| 2_1^+ \rangle$ matrix element on the γ deformation parameter in the framework of the Davydov-Filippov model [53]. The calculations were performed for the energy of the first excited state in ^{98}Sr equal to the experimental value of 144.2 keV, and $\beta = 0.36$ that reproduced the measured value of $\langle 2_1^+ \| E2 \| 0_1^+ \rangle$ for axial symmetry ($\gamma = 0$ degrees). In order to account for the fact that the $\langle 2_1^+ \| E2 \| 0_1^+ \rangle$ value predicted by the model slightly decreases with increasing γ parameter, the evolution

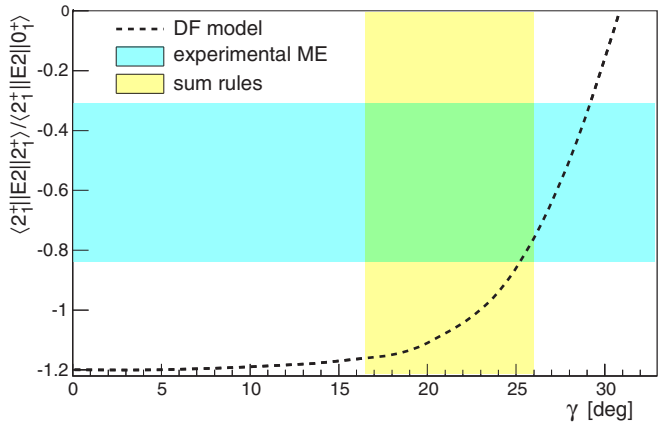

FIG. 11. Diagonal matrix element $\langle 2_1^+\|E2\|2_1^+\rangle$ in ^{98}Sr, normalized to the $\langle 2_1^+\|E2\|0_1^+\rangle$, as a function of the γ deformation parameter. The black dashed line represents the results of the Davydov-Filippov model, the blue shaded area corresponds to the values of matrix elements determined in the present study (with 1σ uncertainty), and the yellow shaded area to the result of the quadrupole sum rules approach for the 0_1^+ state in ^{98}Sr.

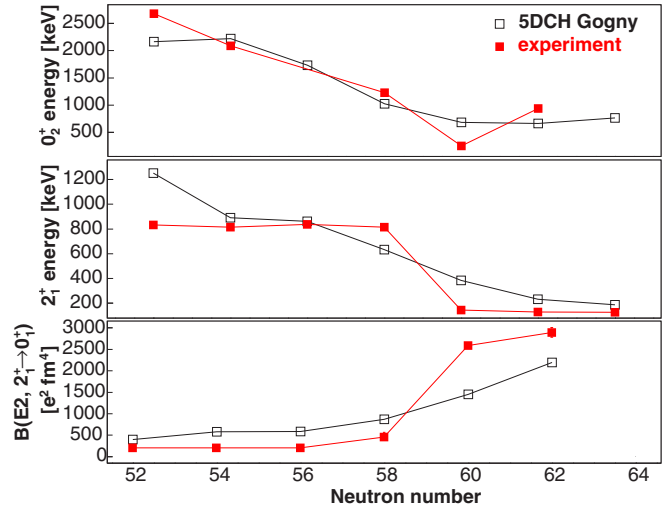

FIG. 12. Comparison between the theoretical (black) and experimental (red) systematics of excitation energies of the 0_2^+ (top) and 2_1^+ (middle) states and the $B(E2,2_1^+ \rightarrow 0_1^+)$ values (bottom). The theoretical values for ^{90,92}Sr are taken from [72]. For most experimental points uncertainties are smaller than the marker size.

of the ratio $\langle 2_1^+\|E2\|2_1^+\rangle/\langle 2_1^+\|E2\|0_1^+\rangle$ is presented in Fig. 11. These results are compared to the values of matrix elements determined in the present study, as well as to the result of the quadrupole sum-rules approach for the ground state in ^{98}Sr. Although the results are not fully consistent, it is clear that γ deformation of about 25 degrees could explain the observed reduction of the quadrupole moment of the 2_1^+ state. However, at the same time, one would expect to observe a low-lying gamma-vibrational 2^+ state, and possibly other members of the gamma band. No candidate for such a structure is known in ^{98}Sr and, as a consequence, the triaxiality of this nucleus remains an open question. It should be noted, however, that predictions of recent beyond-mean-field calculations using a relativistic PC-PK1 interaction [54] are strikingly similar to what is observed experimentally: the ground state is calculated to have a significant γ deformation of about 20°, while the other members of the ground-state band are more axially symmetric ($\gamma \approx 10°$). Although in these calculations the γ degree of freedom clearly influences the structure of ^{98}Sr at low spin, they predict the $K = 2$ band to appear as high as 1.2 MeV, which is not much lower than the measured energy of the first candidate for a 2_3^+ state (1539 keV [27]).

The shape transition at $N = 60$ in the Sr and Zr isotopic chains has been a subject of numerous theoretical works (see for instance Refs. [40,55–69]). Only very few predictions of electromagnetic properties are available, and those are usually limited to $B(E2,2_1^+ \rightarrow 0_1^+)$ values. The theoretical models reproduce the observed onset of deformation qualitatively, but differ in the predictions of deformation parameters and excitation energies at the transition between $N = 58$ and $N = 60$. In calculations restricted to axial symmetry, potential energy surfaces present a shallow spherical minimum at $N = 58$ and deformed minima at $N = 60$ with almost degenerate oblate and prolate configurations. Most of the calculations including the triaxial degree of freedom predict a slightly oblate ground state at $N = 58$, and a strongly deformed prolate shape at $N = 60$. Our measurement suggests rather a weak prolate deformation of the ground state in $N = 58$ ^{96}Sr and a highly deformed prolate ground-state band in ^{98}Sr, with triaxiality being important particularly at low spin. Large-scale conventional shell model calculations performed for the Zr istotopic chain [6] reproduce satisfactorily the low-spin structure and qualitatively the $B(E2,2_1^+ \rightarrow 0_1^+)$ values, but they are, at present, limited to nuclei with $N \leqslant 58$; a much larger valence space using a ^{56}Ni inert core would be required to describe nuclei beyond $N = 58$. Such calculations have, however, recently been achieved with the Monte Carlo shell model approach [7] and were found to successfully reproduce, for the first time, the dramatic increase in $B(E2,2_1^+ \rightarrow 0_1^+)$, indicating the sudden onset of deformation, in the Zr isotopic chain at $N = 60$. This, therefore, calls for a more global comparison with our data for the Sr isotopes.

We have performed beyond-mean-field calculations using the Gogny D1S interaction [70,71] in a five-dimensional collective Hamiltonian (5DCH) formalism [72] for the ^{96}Sr and ^{98}Sr isotopes in order to obtain spectroscopic quadrupole moments and reduced transition probabilities for all states observed experimentally. The comparison of the calculated $B(E2)$ and Q_s with the experimental values is presented in Refs. [22,23]. Here, we present these results in the context of the entire Sr isotopic chain, provide some details on the procedure applied to assign levels to specific bands, compare them to predictions from other models for ^{96,98}Sr, and finally present the theoretical results concerning monopole strengths in ^{96,98}Sr.

The systematics of the calculated and measured excitation energies of the 2_1^+ and 0_2^+ states and the $B(E2,2_1^+ \rightarrow 0_1^+)$ values as a function of the neutron number is presented in Fig. 12. The theoretical calculation reproduces the onset of collectivity beyond $N = 60$, but its character is more gradual

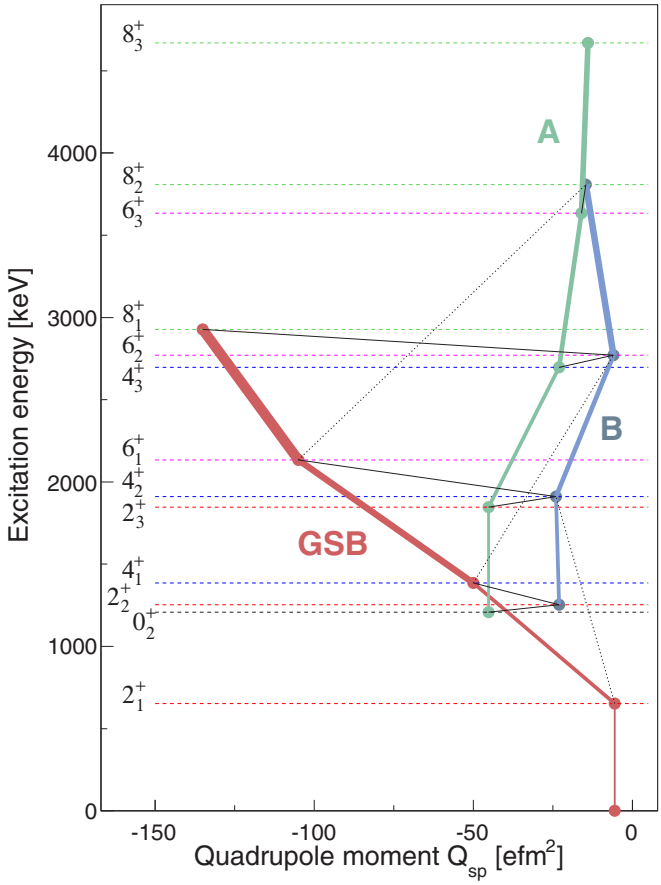

FIG. 13. Assignment of calculated levels in ^{96}Sr to specific bands. All $J \rightarrow J-2$ transitions with $B(E2)$ values higher than 10 e^2fm^4 are marked with lines. Dotted lines correspond to $B(E2)$ values lower than 100 e^2fm^4, while for those higher than 100 e^2fm^4 solid lines are used, and their width is proportional to $B(E2;\ J \rightarrow J-2)$. Energies of 0_2^+ and 2_3^+ levels are offset by 40 keV for clarity. For the same reason spectroscopic moments of 0^+ states are presented as being equal to those of the corresponding 2^+ states. Bands are labeled as in Refs. [22,23].

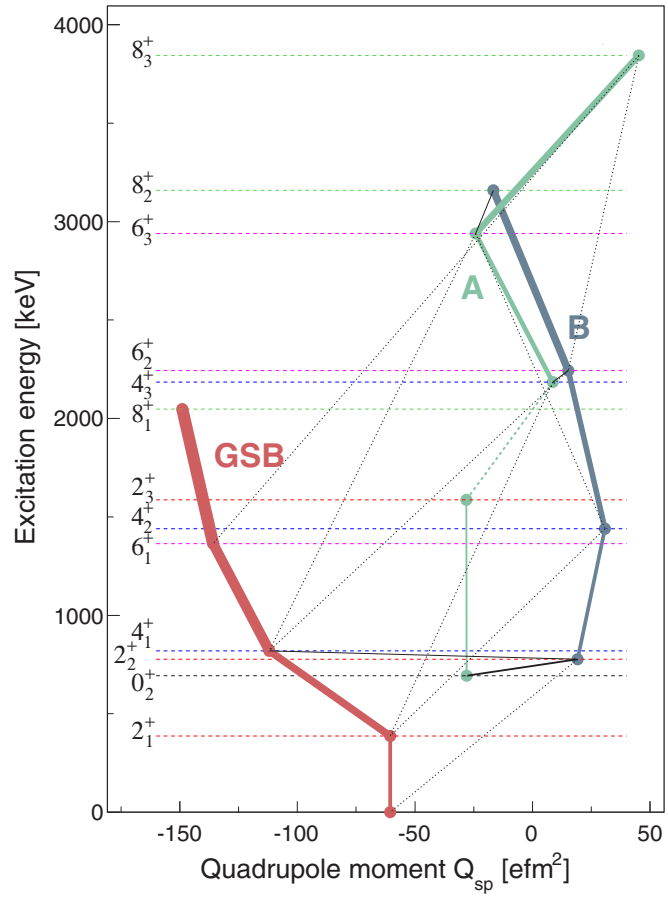

FIG. 14. Same as Fig. 13 but for ^{98}Sr. Energies of 2_2^+ and 4_3^+ levels are offset by 40 keV for clarity.

than the experimentally observed sharp rise at $N = 60$. This is visible both in the calculated energies of the 2_1^+ state, as well as in the $B(E2,2_1^+ \rightarrow 0_1^+)$ values. The energy of the first excited 0^+ state is rather well reproduced, except at $N = 60$, as discussed in Refs. [22,23] and in following paragraphs of the present paper.

It should be noted that in the 5DCH approach band structures do not appear naturally, as states are calculated in groups of the same spin. We present here a graphical method to assign calculated states to specific bands that was used to construct the level schemes presented in Ref. [22,23]. The excited states obtained from the calculations are grouped according to the evolution of their spectroscopic quadrupole moments with spin and reduced transition strengths between states. The method is illustrated in Fig. 13 for ^{96}Sr and in Fig. 14 for ^{98}Sr. The calculated excitation energies are plotted on the y axis and the corresponding spectroscopic quadrupole moments on the x axis. The lines represent $J \rightarrow J-2$ transitions with $B(E2)$ values higher than 10 e^2fm^4, and their width is proportional to the $B(E2)$ value. For presentation purpose, we assign to each 0^+ state the spectroscopic quadrupole moment of the 2^+ state attributed to the same band. From the smooth evolution of the excitation energies, the spectroscopic quadrupole moments and the transition strength between states, band structures can be identified for both isotopes. The corresponding sequences are labeled as in Refs. [22,23]. In ^{96}Sr, the ground state band is characterized by an increase in collectivity, starting from a weakly deformed first 2^+ state and reaching large prolate deformation for the 8_1^+ state. Two other band structures clearly emerge. A comparison of the $B(E2,0_2^+ \rightarrow 2_2^+)$ and $B(E2,0_2^+ \rightarrow 2_3^+)$ transition strengths (600 e^2fm^4 versus 1200 e^2fm^4) leads to the assignment of the 0_2^+ state as a band head of the band (A), while the structure (B) appears on top of the 2_2^+ state. A large $K = 2$ contribution calculated for the band (B) is consistent with smaller spectroscopic quadrupole moments in this structure as compared to those in the (A) band, which presents a larger contribution of $K = 0$. It is worth noting that the level spacing of bands (A) and (B) is quite similar, and calculated $B(E2;(J+2)_B \rightarrow (J)_A)$ do not change a great deal with spin. The same conclusion can be drawn for $(J+2)_{GSB} \rightarrow (J)_B$ transitions. In ^{98}Sr, the ground state band shows a similar evolution with spin to that of the ground-state band in ^{96}Sr with, however, a larger moment of inertia and higher spectroscopic quadrupole moments,

TABLE VII. Reduced transition probabilities in ^{96}Sr, expressed in Weisskopf units, and monopole transition strengths $\rho^2(E0)$ between 0^+ states. Experimental results, including the newly measured $B(E2; 2_1^+ \to 0_1^+)$, are compared with those calculated within the beyond-mean-field approach with a five-dimensional collective Hamiltonian and the Gogny D1S force (present study) and using the complex excited VAMPIR approach [40].

I_1^π	I_2^π	$B(E2, I_1 \to I_2)$ (W.u.)		
		Eexperiment	5DCH (Gogny)	Excited VAMPIR
2_1^+	0_1^+	$17.3^{+4.0}_{-3.2}$	32	30
4_1^+	2_1^+		63	68
0_2^+	2_1^+	15.3(16) [10]	58	83
0_3^+	2_1^+	0.028(11) [11]		
2_2^+	2_1^+	>8.9 [10]	62	65
4_1^+	2_2^+		13	7
4_2^+	2_2^+		57	73
4_2^+	4_1^+		49	47
			$\rho^2(E0)$ ($\times 10^3$)	
0_2^+	0_1^+		106	66
0_3^+	0_1^+		22	
0_3^+	0_2^+	185(50) [13]	95	9

TABLE VIII. Reduced transition probabilities in ^{98}Sr, expressed in Weisskopf units, and monopole transition strengths $\rho^2(E0)$ between 0^+ states. Present experimental results are compared to those calculated within the beyond-mean-field approach with a five-dimensional collective Hamiltonian and the Gogny D1S force (present study) and relativistic PC-PK1 interaction [54].

I_1^π	I_2^π	$B(E2, I_1 \to I_2)$ (W.u.)		
		Experiment	5DCH (Gogny)	5DCH (PC-PK1)
2_1^+	0_1^+	96 (3)	54	73.5
4_1^+	2_1^+	129^{+8}_{-7}	110	162
6_1^+	4_1^+	175^{+17}_{-14}	150	196
8_1^+	6_1^+	123^{+19}_{-14}	173	211
2_2^+	0_2^+	13 (2)	28	39.2
0_2^+	2_1^+	61 (5)	120	195[a]
2_2^+	0_1^+	0.77 (13)	0.07	
2_2^+	2_1^+	$0.61^{+0.22}_{-0.30}$	0.78	
2_2^+	4_1^+	4^{+4}_{-2}	19.4	
			$\rho^2(E0)$ ($\times 10^3$)	
0_2^+	0_1^+	53(5) [21]	179	117
0_3^+	0_1^+		40	
0_3^+	0_2^+		75	

[a]Calculated from $B(E2; 2_1^+ \to 0_2^+) = 39.1$ W.u. [54].

hence underlining its rotational character. As described in Refs. [22,23], the assignment of excited states to specific bands is more difficult in ^{98}Sr. The (B) sequence appears as a $K = 2$ band with large $B(E2)$ values between states, and the (A) band is much less collective. Both bands have very small spectroscopic quadrupole moments in contrast to the ground-state band, consistent with the shape coexistence scenario.

Finally, it is worth pointing out that the general picture of three structures is similar for the two isotopes, although the moments of inertia and magnitudes of transition probabilities and quadrupole moments obviously differ. In both cases, the deformation of the ground-state band quickly develops with spin, while the two other structures have much lower quadrupole moments. This effect may be related to the fact that the ground-state band corresponds to the absolute minimum of the potential energy surface for each angular momentum projection while the other structures are built on secondary minima.

In the case of ^{96}Sr, our results can be further compared to those obtained using the complex excited VAMPIR approach with a realistic effective interaction based on the Bonn A potential in a large model space [40]. These calculations predict a $B(E2, 2_1^+ \to 0_1^+)$ value that is similar to the result of our beyond-mean-field calculation, and the spectroscopic quadrupole moment of the 2_1^+ state equal to $+0.095$ eb. Both theoretical values were translated into matrix elements and plotted along the χ^2 surface in Fig. 7 for comparison. It is interesting to note that both models reproduce correctly the low Q_s, but tend to overestimate the $B(E2, 2_1^+ \to 0_1^+)$ value. A more complete comparison of transition probabilities resulting from both model approaches is presented in Table VII. Again, the predictions of these two fundamentally different models are remarkably consistent and call for a systematic comparison along isotopic chains between the two models. A notable difference is observed, however, for the spectroscopic quadrupole moments in the side band. Our present calculations predict a rapid and constant increase of quadrupole moments with spin in the ground-state band, reaching -104 $e$fm^2 for the 6_1^+ state, and considerably lower values for the first side band, decreasing with spin to -6 $e$fm^2 for 6_2^+ [22,23]. In contrast, the Excited VAMPIR calculations [40] yield a very large negative value of -120 $e$fm^2 for the 6_2^+ state, and further increase of spectroscopic quadrupole moments with spin in the side band. Unfortunately, the experimental information on transition probabilities and quadrupole moments of low-lying states in ^{96}Sr is scarce, and these predictions cannot be compared to measured values.

For ^{98}Sr, recent beyond-mean-field calculations using a relativistic PC-PK1 interaction [54] predict transition probabilities in the ground-state band that are slightly higher than the experimental results; see Table VIII. The collectivity of the band built on the 0_2^+ state is strongly overestimated, as well as the $0_2^+ \to 2_1^+$ transition strength. It should be noted, however, that the excitation energy of the 0_2^+ state has been very well reproduced by this model (216 keV, as compared to the experimental value of 215 keV), better than in the case of earlier calculations by the same group using Sly4 interaction (590 keV, [69]) and our present calculations that yield 692 keV.

Finally, monopole transition strengths $\rho^2(E0)$ in ^{96,98}Sr were calculated between the collective states obtained within the 5DCH approach up to spin 8. The results are presented in Table IX, and in addition those for $J = 0$ are compared to available experimental data and excited VAMPIR [40] and 5DCH (PC-PK1) [54] predictions in Tables VII and VIII. In ^{96}Sr, a large transition strength is predicted between the 0_2^+ state and the ground state by both our calculation and the VAMPIR approach. However, the $0_2^+ \to 0_1^+$ $E0$ transition

TABLE IX. Monopole transition strengths in ^{96,98}Sr, calculated within the beyond-mean-field approach with a five-dimensional collective Hamiltonian and the Gogny D1S force.

^{96}Sr, $\rho^2(E0)$ ($\times 10^3$)												
	0_1^+	0_2^+		2_1^+	2_2^+		4_1^+	4_2^+		6_1^+	6_2^+		8_1^+	8_2^+
0_2^+	106		2_2^+	28		4_2^+	83		6_2^+	82		8_2^+	60	
0_3^+	22	95	2_3^+	117	65	4_3^+	113	43	6_3^+	89	32	8_3^+	44	44
^{98}Sr, $\rho^2(E0)$ ($\times 10^3$)												
	0_1^+	0_2^+		2_1^+	2_2^+		4_1^+	4_2^+		6_1^+	6_2^+		8_1^+	8_2^+
0_2^+	179		2_2^+	81		4_2^+	43		6_2^+	27		8_2^+	20	
0_3^+	40	75	2_3^+	120	1	4_3^+	0	16	6_3^+	0	27	8_3^+	2	32

has not been observed experimentally, which suggests to the contrary a very low $\rho^2(E0)$. Our calculations predict a significant transition strength between the 0_3^+ and the 0_1^+ states in contrast to the VAMPIR calculation and the experimental data. The experimental $E0$ strength for the $0_3^+ \rightarrow 0_2^+$ transition in ^{96}Sr ranks among the strongest known beyond $A > 40$. Our calculations also predict a large $\rho^2(E0)$ value for this transition, in contrast to the VAMPIR calculations that yielded a rather small $E0$ strength. In fact, our calculations also predict large $\rho^2(E0)$ values, generally greater than 3×10^{-2}, for all transitions between $J > 0$ states. This is illustrated by Fig. 15, which presents calculated $E0$ transitions strengths between three bands in ^{96}Sr, defined as in Fig. 13. In Fig. 15, all transitions with $\rho^2(E0)$ values greater than 10^{-2} are marked with lines, and their width is proportional to the $\rho^2(E0)$ value. In this representation one can easily see that all three calculated states of the same spin are always coupled by significant $E0$ transitions, which suggests complex mixing between these states that decreases slowly with spin.

In ^{98}Sr, the experimental $\rho^2(E0)$ value of 0.053(5) for the $0_2^+ \rightarrow 0_1^+$ transition can be compared to about 0.02 obtained using the 5DCH (Sly4) approach [69], 0.117 resulting from the 5DCH (PC-PK1) calculation [54] and our present theoretical value of 0.178. All calculations predict considerable $\rho^2(E0)$ values, consistent with the experimental observation. In addition, our calculations predict a 0_3^+ state coupled by strong $E0$ transitions to both the ground state and the first exicted 0^+ state. For spin $J = 2$, a very large $E0$ strength is calculated between the rotational 2_1^+ state and both the 2_2^+ γ band head and the 2_3^+ state. The $E0$ transition strengths rapidly decrease

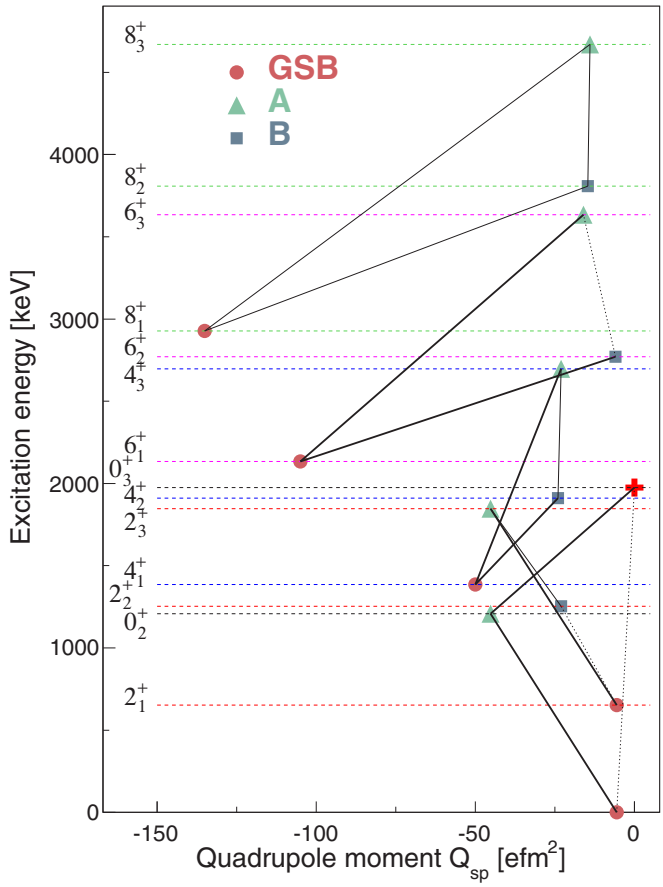

FIG. 15. Same as Fig. 13 but for calculated $E0$ transition strengths in ^{96}Sr. All transitions with $\rho^2(E0)$ values higher than 10^{-2} are marked with lines. Dotted lines correspond to $\rho^2(E0)$ values lower than 4×10^{-2}, while for those higher than 4×10^{-2} solid lines are used, and their width is proportional to $\rho^2(E0)$. Bands are labeled as in Refs. [22,23] and Fig. 13. The 0_3^+ state, not attributed to any of these bands, is marked with a red cross at $Q_{sp} = 0$ and offset by 30 keV for clarity.

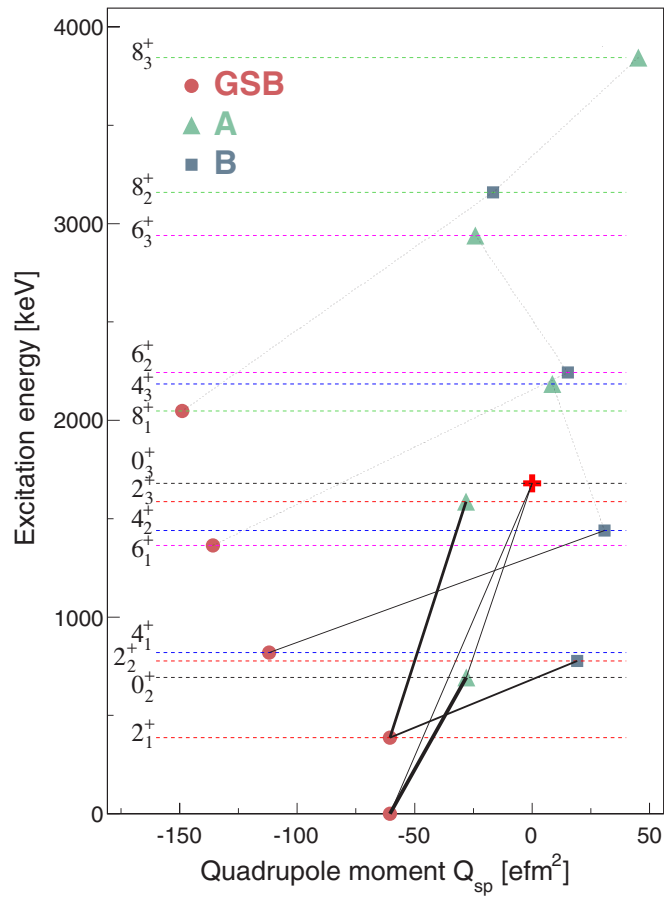

FIG. 16. Same as Fig. 15 but for ^{98}Sr. Energy of the 0_3^+ level is offset by 60 keV for clarity.

with spin, and, moreover, above spin 2 they remain important only between the rotational ground-state band and the γ band (B), and between the bands (A) and (B). In contrast, all $E0$ strengths between the ground-state band and the band (A) are below 2×10^{-3}. This is illustrated in Fig. 16, which clearly shows a transition pattern of monopole transition strengths very different to that obtained for ^{96}Sr (Fig. 15), with strong $E0$ transitions present only at low spin.

VI. SUMMARY

Shape coexistence in neutron-rich strontium isotopes at $N = 60$ was studied in low-energy Coulomb excitation experiments using radioactive ^{96}Sr and ^{98}Sr beams from the REX-ISOLDE facility, CERN. Reduced transition probabilities and spectroscopic quadrupole moments for low-lying states in ^{96,98}Sr were extracted from the measured γ-ray yields. Additionally, new short-lived excited states in the beam contaminant, ^{98}Rb, are proposed.

In ^{96}Sr, the spectroscopic quadrupole moment of the first 2^+ state was found to be small and negative, corresponding to a weak prolate deformation. In ^{98}Sr, the large and negative spectroscopic quadrupole moments in the ground state band demonstrate its prolate rotational character, while the value close to zero obtained for the 2^+_2 state confirms the shape coexistence between highly-deformed prolate and spherical configurations in this nucleus. The comparison of the $B(E2)$ values and the spectroscopic quadrupole moments between the 2^+_1 state in ^{96}Sr and the 2^+_2 state in ^{98}Sr underlines their similarity and further supports the shape inversion when crossing the $N = 60$ line. The reduced $E2$ matrix elements were interpreted in a phenomenological two band mixing model. The results support the weak mixing scenario between prolate and spherical configurations in the wave functions of the 0^+ states in ^{98}Sr, in spite of their proximity in energy. The increase of the spectroscopic quadrupole moments observed beyond the 2^+_1 state can be attributed to a certain level of triaxiality in the ground state. This interpretation is further supported by the results of the quadrupole sum rules method applied to the 0^+ states in ^{98}Sr, where the values of the quadrupole invariant $\langle \mathcal{Q}^3 \cos(3\delta) \rangle$ for both states suggest a significant degree of triaxiality.

The experimental results were compared to 5DCH calculations using the Gogny D1S interaction, which reproduce the shape coexistence between deformed and spherical configurations in ^{96}Sr and ^{98}Sr and the change of the ground state deformation at $N = 60$. For ^{96}Sr, a comparison was also possible with the predictions of the excited VAMPIR model, while for ^{98}Sr with those obtained within the 5DCH approach with the relativistic PC-PK1 force. New theoretical results on monopole transition strengths in ^{96,98}Sr are also presented and discussed. These call for a detailed comparison with experimental information on $E0$ transition strengths in ^{96,98}Sr, which is at present very limited.

Due to the low collectivity of the ground-state band in ^{96}Sr, the presumably highly deformed structures built on the $0^+_{2,3}$ states could not be investigated. The measurement of the spectroscopic quadrupole moments of the 2^+_2 and 2^+_3 states in ^{96}Sr and corresponding results in the Zr and Kr isotopes remain a challenge for future radioactive-ion beam facilities.

ACKNOWLEDGMENTS

S.P. and H.G. appreciate illuminating discussions with Jean Libert and thank him for his contribution to the theoretical interpretation. M.Z. acknowledges fruitful discussions with Jacek Dobaczewski. We would like to thank the technical teams at ISOLDE for their support and the MINIBALL Collaboration for their work in setting up and in the continued operation of the MINIBALL detector array. The work was partially supported by the German BMBF under Contracts No. 05P15PKCIA, No. 06 KY 205, No. 06KY9136I, No. 05P12PKFNE, and No. 05P12RDCIB, by the Verbundprojekt 05P2015, by the Norwegian Research Council under Contracts No. 180663 and No. 213442, the Research Foundation Flanders (FWO), Belgian Science Office (IUAP), by the UK Science & Technology Facilities Council, by the Polish National Science Centre under Contracts No. DEC-2013/10/M/ST2/00427 and UM0-2013/08/M/ST2/0025 (LEA-COPIGAL), by the Polish-French Collaboration COPIN-IN2P3 (Project No. 06-121), and by the Swedish Research Council under Contracts No. VR 2009-3939 and No. VR 2003-2727. A.C.L. acknowledges funding from ERC-STG-2014 under Grant Agreement No. 637686 and G.M.T acknowledges funding from the Norwegian Research Council under Contract No. 222287. The authors also acknowledge for its support the European Union, Seventh Framework Programme through ENSAR, Contract No. 262010. J.P. acknowledges support of the Marie Curie Intra-European Fellowship of the European Community, Seventh Framework Programme under Contract No. PIEF-GA-2008-219175.

[1] S. A. Johansson, Nucl. Phys. **64**, 147 (1965).
[2] G. Audi *et al.*, Chin. Phys. C **36**, 1287 (2012).
[3] S. Naimi *et al.*, Phys. Rev. Lett. **105**, 032502 (2010).
[4] M. Albers *et al.*, Phys. Rev. Lett. **108**, 062701 (2012).
[5] K. Heyde and J. L. Wood, Rev. Mod. Phys. **83**, 1467 (2011).
[6] K. Sieja, F. Nowacki, K. Langanke, and G. Martinez-Pinedo, Phys. Rev. C **79**, 064310 (2009).
[7] T. Togashi, Y. Tsunoda, T. Otsuka, and N. Shimizu, Phys. Rev. Lett. **117**, 172502 (2016).
[8] O. Sorlin and M.-G. Porquet, Prog. Part. Nucl. Phys. **61**, 602 (2008).
[9] S. M. Lenzi, F. Nowacki, A. Poves, and K. Sieja, Phys. Rev. C **82**, 054301 (2010).
[10] H. Mach *et al.*, Nucl. Phys. A **523**, 197 (1991).
[11] G. Jung, B. Pfeiffer, L. J. Alquist, H. Wollnik, P. Hungerford, S. M. Scott, and W. D. Hamilton, Phys. Rev. C **22**, 252 (1980).
[12] K. Kawade *et al.*, Z. Phys. A **304**, 293 (1982).
[13] G. Lhersonneau *et al.*, Phys. Rev. C **49**, 1379 (1994).

[14] H. Mach *et al.*, Phy. Lett. B **230**, 21 (1989).
[15] H. Ohm, G. Lhersonneau, K. Sistemich, B. Pfeiffer, and K.-L. Kratz, Z. Phys. A **327**, 483 (1987).
[16] H. Mach *et al.*, Nucl. Instrum. Methods Phys. Res., Sect. A **280**, 49 (1989).
[17] G. Lhersonneau, B. Pfeiffer, R. Capote, J. M. Quesada, H. Gabelmann, and K.-L. Kratz, Phys. Rev. C **65**, 024318 (2002).
[18] A. G. Smith *et al.*, Phys. Rev. Lett. **77**, 1711 (1996).
[19] A. G. Smith, J. L. Durell, W. R. Phillips, W. Urban, P. Sarriguren, and I. Ahmad, Phys. Rev. C **86**, 014321 (2012).
[20] F. Schussler *et al.*, Nucl. Phys. A **339**, 415 (1980).
[21] J. Park *et al.*, Phys. Rev. C **93**, 014315 (2016).
[22] E. Clément *et al.*, Phys. Rev. Lett. **116**, 022701 (2016).
[23] E. Clément, M. Zielińska, A. Görgen, W. Korten, S. Péru, J. Libert, H. Goutte, S. Hilaire, B. Bastin, C. Bauer, A. Blazhev, N. Bree, B. Bruyneel, P. A. Butler, J. Butterworth, P. Delahaye, A. Dijon, D. T. Doherty, A. Ekström, C. Fitzpatrick, C. Fransen, G. Georgiev, R. Gernhäuser, H. Hess, J. Iwanicki, D. G. Jenkins, A. C. Larsen, J. Ljungvall, R. Lutter, P. Marley, K. Moschner, P. J. Napiorkowski, J. Pakarinen, A. Petts, P. Reiter, T. Renstrøm, M. Seidlitz, B. Siebeck, S. Siem, C. Sotty, J. Srebrny, I. Stefanescu, G. M. Tveten, J. Van de Walle, M. Vermeulen, D. Voulot, N. Warr, F. Wenander, A. Wiens, H. De Witte, and K. Wrzosek-Lipska, Phys. Rev. Lett. **117**, 099902 (2016).
[24] N. Warr *et al.*, Eur. Phys. J A **49**, 1 (2013).
[25] D. Cline, Annu. Rev. Nucl. Part. Sci. **36**, 683 (1986).
[26] J. Van de Walle *et al.*, Eur. Phys. J A **42**, 401 (2009).
[27] B. Singh and Z. Hu, Nucl. Data Sheets **98**, 335 (2003).
[28] E. Clément, A. Görgen, A. Dijon, G. de France, B. Bastin, A. Blazhev, N. Bree, P. Butler, P. Delahaye, A. Ekstrom, G. Georgiev, N. Hasan, J. Iwanicki, D. Jenkins, W. Korten, A.C. Larsen, J. Ljungvall, K. Moschner, P. Napiorkowski, J. Pakarinen, A. Petts, T. Renstrom, M. Seidlitz, S. Siem, C. Sotty, J. Srebrny, I. Stefanescu, G. M. Tveten, J. Van de Walle, N. Warr, K. Wrzosek-Lipska, M. Zielińska, C. Bauer, B. Bruyneel, J. Butterworth, C. Fitzpatrick, C. Fransen, R. Gernhäuser, H. Hess, R. Lutter, P. Marley, P. Reiter, B. Siebeck, M. Vermeulen, A. Wiens, and H. De Witte, EPJ Web Conf. **62**, 01003 (2013).
[29] A. Dewald, S. Harissopulos, and P. von Brentano, Z. Phys. A **334**, 163 (1989).
[30] J. A. Pinston, J. Genevey, R. Orlandi, A. Scherillo, G. S. Simpson, I. Tsekhanovich, W. Urban, H. Faust, and N. Warr, Phys. Rev. C **71**, 064327 (2005).
[31] F. K. Wohn, J. C. Hill, J. A. Winger, R. F. Petry, J. D. Goulden, R. L. Gill, A. Piotrowski, and H. Mach, Phys. Rev. C **36**, 1118 (1987).
[32] S. Bottoni *et al.*, Phys. Rev. C **92**, 024322 (2015).
[33] C. M. Folden, A. S. Nettleton, A. M. Amthor, T. N. Ginter, M. Hausmann, T. Kubo, W. Loveland, S. L. Manikonda, D. J. Morrissey, T. Nakao, M. Portillo, B. M. Sherrill, G. A. Souliotis, B. F. Strong, H. Takeda, and O. B. Tarasov, Phys. Rev. C **79**, 064318 (2009).
[34] D. Kameda, T. Kubo, T. Ohnishi, K. Kusaka, A. Yoshida, K. Yoshida, M. Ohtake, N. Fukuda, H. Takeda, K. Tanaka, N. Inabe, Y. Yanagisawa, Y. Gono, H. Watanabe, H. Otsu, H. Baba, T. Ichihara, Y. Yamaguchi, M. Takechi, S. Nishimura, H. Ueno, A. Yoshimi, H. Sakurai, T. Motobayashi, T. Nakao, Y. Mizoi, M. Matsushita, K. Ieki, N. Kobayashi, K. Tanaka, Y. Kawada, N. Tanaka, S. Deguchi, Y. Satou, Y. Kondo, T. Nakamura, K. Yoshinaga, C. Ishii, H. Yoshii, Y. Miyashita, N. Uematsu, Y. Shiraki, T. Sumikama, J. Chiba, E. Ideguchi, A. Saito, T. Yamaguchi, I. Hachiuma, T. Suzuki, T. Moriguchi, A. Ozawa, T. Ohtsubo, M. A. Famiano, H. Geissel, A. S. Nettleton, O. B. Tarasov, D. Bazin, B. M. Sherrill, S. L. Manikonda, and J. A. Nolen, Phys. Rev. C **86**, 054319 (2012).
[35] T. Procter, J. Behr, J. Billowes, F. Buchinger, B. Cheal, J. Crawford, J. Dilling, A. Garnsworthy, A. Leary, C. Levy, E. Mané, M. Pearson, O. Shelbaya, M. Stolz, W. Al Tamimi, and A. Voss, Eur. Phys. J. A **51**, 1 (2015).
[36] H. Mach, F. K. Wohn, M. Moszyński, R. L. Gill, and R. F. Casten, Phys. Rev. C **41**, 1141 (1990).
[37] T. Czosnyka, D. Cline, and C. Y. Wu, Bull. Am. Phys. Soc. **28**, 745 (1983).
[38] GOSIA User's Manual, http://www.slcj.uw.edu.pl/gosia/
[39] M. Zielińska, L. P. Gaffney, K. Wrzosek-Lipska, E. Clément, T. Grahn, N. Kesteloot, P. Napiorkowski, J. Pakarinen, P. Van Duppen, and N. Warr, Eur. Phys. J. A **52**, 1 (2016).
[40] A. Petrovici, Phys. Rev. C **85**, 034337 (2012).
[41] E. Clément *et al.*, Phys. Rev. C **75**, 054313 (2007).
[42] K. Wrzosek-Lipska *et al.*, Phys. Rev. C **86**, 064305 (2012).
[43] N. Bree *et al.*, Phys. Rev. Lett. **112**, 162701 (2014).
[44] T. Kibédi, T. Burrows, M. Trzhaskovskaya, P. Davidson, and C. N. Jr., Nucl. Instrum. Methods Phys. Res., Sect. A **589**, 202 (2008).
[45] K. Becker *et al.*, Z. Phys. A **319**, 193 (1984).
[46] G. J. Kumbartzki *et al.*, Phys. Rev. C **89**, 064305 (2014).
[47] A. Smith *et al.*, Phys. Lett. B **591**, 55 (2004).
[48] J. Srebrny *et al.*, Int. J. Mod. Phys. E **20**, 422 (2011).
[49] W. Andrejtscheff and P. Petkov, Phys. Lett. B **329**, 1 (1994).
[50] C. Y. Wu, H. Hua, and D. Cline, Phys. Rev. C **68**, 034322 (2003).
[51] L. Grente, Ph.D. thesis, Université Paris XI - Paris Sud, UFR Orsay, 2014 (unpublished).
[52] L. Grente *et al.*, EPJ Web Conf. **62**, 01002 (2013).
[53] A. Davydov and G. Filippov, Nucl. Phys. **8**, 237 (1958).
[54] J. Xiang, J. M. Yao, Y. Fu, Z. H. Wang, Z. P. Li, and W. H. Long, Phys. Rev. C **93**, 054324 (2016).
[55] D. Arseniev *et al.*, Nucl. Phys. A **139**, 269 (1969).
[56] P. Federman and S. Pittel, Phys. Rev. C **20**, 820 (1979).
[57] A. Kumar and M. R. Gunye, Phys. Rev. C **32**, 2116 (1985).
[58] S. Michiaki and A. Akito, Nucl. Phys. A **515**, 77 (1990).
[59] J. Skalski *et al.*, Nucl. Phys. A **559**, 221 (1993).
[60] A. Baran and W. Höhenberger, Phys. Rev. C **52**, 2242 (1995).
[61] G. Lalazissis *et al.*, Nucl. Phys. A **586**, 201 (1995).
[62] J. Skalski *et al.*, Nucl. Phys. A **617**, 282 (1997).
[63] A. Holt, T. Engeland, M. Hjorth-Jensen, and E. Osnes, Phys. Rev. C **61**, 064318 (2000).
[64] H. Zhang *et al.*, Eur. Phys. J. A **30**, 519 (2006).
[65] T. Rząca-Urban, K. Sieja, W. Urban, F. Nowacki, J. L. Durell, A. G. Smith, and I. Ahmad, Phys. Rev. C **79**, 024319 (2009).
[66] R. Rodriguez-Guzman *et al.*, Phy. Lett. B **691**, 202 (2010).
[67] Y.-X. Liu *et al.*, Nucl. Phys. A **858**, 11 (2011).
[68] J. Xiang *et al.*, Nucl. Phys. A **873**, 1 (2012).
[69] H. Mei, J. Xiang, J. M. Yao, Z. P. Li, and J. Meng, Phys. Rev. C **85**, 034321 (2012).
[70] J. Dechargé and D. Gogny, Phys. Rev. C **21**, 1568 (1980).
[71] J. Berger *et al.*, Comput. Phys. Commun. **63**, 365 (1991).
[72] J. P. Delaroche *et al.*, Phys. Rev. C **81**, 014303 (2010).